Applied Energy 314 (2022) 118906

Contents lists available at ScienceDirect

Applied Energy

journal homepage: www.elsevier.com/locate/apenergy

Data-driven energy management of isolated power systems under rapidly varying operating conditions[☆,☆☆,★]

Spyridon Chapaloglou [a,*], Damiano Varagnolo [b,e], Francesco Marra [c], Elisabetta Tedeschi [a,d]

[a] Department of Electric Power Engineering, Norwegian University of Science and Technology, O.S. Bragstads Plass 2 E, 7034 Trondheim, Norway
[b] Department of Engineering Cybernetics, Norwegian University of Science and Technology, O.S. Bragstads Plass 2 E, 7034 Trondheim, Norway
[c] Equinor R&T Electrical Technology department, Arkitekt Ebbels 10, 7005, Trondheim, Norway
[d] Department of Industrial Engineering, University of Trento, Via Sommarive, 9, 38123 Povo, Italy
[e] Department of Information Engineering, University of Padova, Via 8 Febbraio, 2, 35122 Padova, Italy

GRAPHICAL ABSTRACT

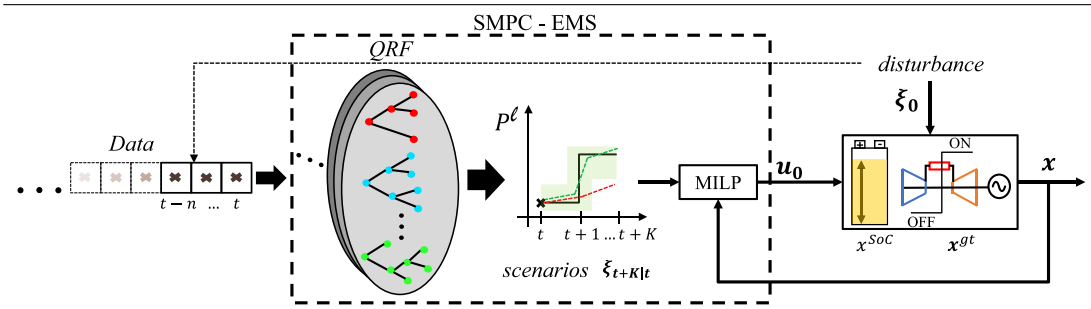

ARTICLE INFO

Keywords:
Stochastic model predictive control
Quantile regression
Random forests
Isolated power systems
Offshore wind power
Energy storage
Mixed-integer linear programming
Economic MPC

ABSTRACT

We propose an energy management algorithm for isolated industrial power systems that integrate uncertain renewable generation and energy storage. The proposed strategy is designed to ensure sustainable and cost-effective operations by managing the energy flows in the grid, and is structured so to cope with: *(1)* high levels of renewable power penetration, and *(2)* load profiles characterized by non-smooth patterns and irregular events (i.e., events such as those occurring from connections/disconnections of large scale equipment, or from large wind speed ramps). The proposed algorithm leverages a stochastic economic model predictive control (MPC) scheme capable of dealing simultaneously with the dispatch and scheduling of the local generation units. More precisely, the scheme embeds a mixed-integer linear programming (MILP) optimal control policy formulation together with a stochastic programming approach. Moreover, the optimization problem accounts for multiple techno-economical objectives, such as minimization of operational costs, battery degradation, and non-utilized energy. We test the algorithm on a case study of an isolated offshore Oil & Gas platform producing energy onsite with conventional gas turbines and a local wind farm, while integrating a battery energy storage

☆ Project/research funded by VISTA - a basic research program in collaboration between The Norwegian Academy of Science and Letters, and Equinor, plus BRU21, NTNU's Research and Innovation Program on Digital and Automation Solutions for the Oil and Gas Industry.
☆☆ This scientific paper was supported by the Onassis Foundation - Scholarship ID: F ZP 056-1/2019-2020.
★ This project has received funding from the European Union's Horizon 2020 research and innovation programme under the Marie Skłodowska-Curie grant agreement No. 956433 (H2020-MSCA-ITN-2020 , Innovative Tools for Cyber-Physical Energy Systems - InnoCyPES).
* Corresponding author.
E-mail addresses: spyridon.chapaloglou@ntnu.no (S. Chapaloglou), damiano.varagnolo@ntnu.no (D. Varagnolo), fmarr@equinor.com (F. Marra), elisabetta.tedeschi@ntnu.no (E. Tedeschi).

https://doi.org/10.1016/j.apenergy.2022.118906
Received 23 November 2021; Received in revised form 28 January 2022; Accepted 5 March 2022
Available online 25 March 2022
0306-2619/© 2022 The Authors. Published by Elsevier Ltd. This is an open access article under the CC BY license (http://creativecommons.org/licenses/by/4.0/).

system. The results show that the proposed approach can issue ensemble predictions that successfully capture the potential irregular variations just by using recent past information of the associated random variable, even when no particular sudden events are anticipated in the near-future (i.e., step changes/trend reversals). In this way, the approach provides useful future information for the optimal management of the grid. This effect is numerically quantified via simulations that compare the performance of the proposed stochastic optimization approach against its deterministic MPC version in several realistic operating conditions. The empirical results suggest that the stochastic version leads to better scheduling of the conventional generators, with up to 12.86% reductions of the operating cost, 2.56% reduction in fuel consumption and emissions, and 35.29% reduction in status transitions (on/off) of the gas turbines, while keeping dumped energy and battery degradation as low as possible.

1. Introduction

Operating resiliently and efficiently islanded microgrids and isolated power systems is believed to require not only integrating energy storage technologies, but also efficiently controlling these [1]. This is especially true for isolated industrial power systems such as remote offshore facilities [2], where specialized energy management systems (EMS) are required. Following the recent trends in the offshore Oil and Gas (O&G) industry [3], battery energy storage systems (BESSs) are expected to significantly contribute towards the decarbonization of the O&G sector. However, to achieve this goal in a cost-efficient and safe way, the particular characteristics of these grids, such as the intermittent load patterns and abrupt load steps [4,5], need to be taken into account. On top of that, integrating renewable energy sources (RES) in these grids adds one more level of complexity due to uncertainty in the power supply. Therefore, appropriate EMS strategies that consider these effects are required. In addition, another important aspect that needs to be captured by the EMS algorithm is the accurate representation of potential time-dependent characteristics of the system's resources, such as BESS degradation [6]. In this way, multiple objectives come together, complicating the calculation of an optimal control policy. Adding then the presence of flexible conventional units with binary operation modes (ON/OFF) makes the energy management optimization problem combinatorial, complicating the numerical search for the optimal solution. As shown in the literature review below, these issues have already been the subject of investigation by the scientific community.

1.1. Literature review

Most of the time, EMS algorithms are formulated either as rule-based strategies or mathematical optimization problems [7–10]. However, such methods do not account for uncertainty in the operating conditions. Recent trends have suggested the consideration of stochastic optimization techniques [1] together with advanced probabilistic forecasting [11,12]. These two components have indeed shown a good potential in dealing with the energy management specifications/requirements under partially known information. A popular approach in integrating uncertainty in the EMS has indeed been the feedback mechanism provided by the Model Predictive Control (MPC) framework [13–15], which can be further enhanced by using mixed-integer linear programming (MILP) [16–18]. Yet, such formulations still do not explicitly consider the uncertainty of future events. Nevertheless, MPC strategies are especially useful for handling energy management problems when combined with stochastic optimization as in [19,20]. However, for better performance and more realistic modeling, such formulations should also consider battery degradation, as we instead do in this paper.

We shall also note that a common way to express uncertainty in stochastic optimization models is through the use of sample paths, called *scenarios*. To be representative of the true random processes, the marginal distribution of each random variable should describe historical data accurately, and at the same time, the joint distribution should also be modeled accurately enough to capture temporal and multivariate correlations [21,22]. The latter requirement is commonly ensured using Cholesky decompositions [23–25]. However, the distribution of each individual random variable is commonly assumed to follow some kind of typical parametric structure [23,24,26], an assumption that should be avoided when arbitrary load characteristics are considered (such as loads including irregular events). An alternative is to learn these distributions from available data. In [27,28], stochastic load and RES are modeled using discrete values and probability mass functions. However, such formulations are prone to the curse of dimensionality, especially when the number of loads or the RES resources in the system increase.

In other studies, quantile forecasting is used as a data-driven method to generate auto-correlated scenarios [25,29,30]. However, in most studies where probabilistic forecasts are issued for RES uncertainty quantification, e.g., [22,30–32], future information about weather conditions is used as input from specialized Numerical Weather Prediction (NWP) models. In this way, such forecasts heavily depend on the availability of these models, which are limited in time resolution, making the forecasting of sudden irregular events (i.e., step changes/trend reversals) extremely challenging.

Then, by combining probabilistic forecasting with scenarios, stochastic optimization, and MPC, an enhanced class of EMS algorithms emerges (SMPC-EMS). In [14,33–35] such strategies were proposed to optimally manage HVAC equipment in the built environment. In [36] a similar method was proposed for the market-based optimal power dispatch, demonstrating the potential application of SMPC-EMS in the power sector. Then, in [25] an SMPC-EMS was proposed for the economic optimization of a grid-connected microgrid integrating PV power.

As evident from the above analysis, state-of-the-art energy management is achieved by combining advanced forecasting and optimization methods. However, to the best of our knowledge, no integrated SMPC-EMS has been proposed for the management of isolated power systems that are subject to irregular load patterns and rapidly varying renewable generation.

1.2. Statement of contributions

It is now clear that the cost-efficient and environmentally sustainable operation of isolated industrial power systems integrating high amounts of renewable resources combined with dispatchable conventional power generation units, is a challenging problem. This is due to: (1) the combined effects of short-term uncertainties coming from both power generation and consumption sides, and (2) the combinatorial nature of the unit commitment decisions. Limitations related to the existing methods are found mainly in an accurate and adaptive probabilistic description of future disturbances to be used along with predictive control, in capturing irregular events without any prior future knowledge, and in dealing with multiple objectives when both continuous and binary decisions need to be taken for the optimal energy management problem. We thus propose to overcome such limitations by formulating and testing an algorithm that:

1. is capable of better quantifying load uncertainty and sudden operation changes just by using lagged values of the load time-series and has an increased performance in predicting trend reversals in wind power generation compared to point forecasts, again by using just lagged values and no future information (i.e., NWP);
2. is formulated as an optimal feedback control problem through employing a MILP that is numerically solvable, in contrast with other schemes that bypass numerical intractability by means of sub-optimal heuristics;
3. includes multiple objectives in its formulation, considering not only the cost-efficient operation of the system, but also its environmental performance by minimizing the wasted (dumped) energy and the optimal usage of the BESS; and
4. uses a detailed degradation model for the BESS, leading thus to operations that do not over-strain this subsystem.

The remainder of this paper is therefore organized as follows: Section 2 presents how to embed the SMPC-energy management system with forecasting capabilities, Section 3 formulates the optimal control problem, and Section 4 presents the numerical results from the simulations. Finally, Section 5 presents an overall summary of the main findings and some concluding remarks.

2. Disturbance uncertainty quantification through probabilistic forecasting

The objective of this section is to build an auto-regressive model that can effectively predict the occurrence of irregular events such as sudden steps and ramps. This capability is especially important in control strategies with fine time discretizations, especially when model-based predictions are either not available or available at higher time resolutions to the point that interpolating such model-based predictions would lead to missing the steps and ramps of our interest. As an example, this applies to load profiles that are characterized by frequent ON/OFF switching of the equipment: in this case, the exact schedule of on or off states might be unknown in advance, since depending on rapidly changing operating conditions, and interpolating coarse model-based predictions of their operations may lead to missing some of these switches.

In the following two subsections, we thus first propose the forecasting method, and then discuss a sensible way to tune its hyper-parameters.

2.1. Quantile regression forests as auto-regressive models

We propose to use Quantile Regression Forests (QRF), that were introduced in [37] and that, to the best of our knowledge, comprise one of the best-performing supervised learning algorithms for quantile regression [38]. This approach has proven useful in providing probabilistic forecast for both RES [11,22] and load [39] time-series, making it suitable for the application considered here. This method makes use of a random forest (RF) structure – i.e., an ensemble of $|\mathcal{T}|$ trees – and this makes it particularly useful for probabilistic forecasting. This is because, besides the prediction of a point value of the response y as in common regression, the whole distribution of the response can be estimated as a function of the predictor input x.

The method is thus formulated so that, in general, at time t one may use the last $L+1$ measured values[1] as input features $x = \left[P_t, P_{t-1}, \dots, P_{t-L}\right]$ to then estimate the conditional empirical distribution $\hat{F}$ of a particular response value $y \in \mathcal{R}$ as

$$\hat{F}(y \mid X = x) = \sum_{j}^{N} \sum_{t \in \mathcal{T}} \frac{1}{|\mathcal{T}|} w_{tj}(x) \mathbb{1}\{Y_j \le y\}. \tag{1}$$

[1] In our specific field case $L = 5$ is the hyperparameter that empirically led to the best results.

To enhance the reproducibility of our results, we note that here X represents the random input feature taking the specific value x, and Y_j are the values of the random response variable for the N observations. Each observation Y_j, $j = 1, \dots, N$ is instead associated with an input sample X_j that belongs to the dedicated bootstrapped training set of the tree $t \in \mathcal{T}$. Then, for each available observation $j = 1, \dots, N$, a weight $w_{tj}(x)$ is assigned, given the specific (new) input x, indicating the fraction of training samples X_j that belong to the same leaf $\mathcal{S}_t(x)$ (set of values in a terminal node) as the one that the new input x falls in. In other words, it expresses how much each observation Y_j from the set of values in the terminal node where $x \in \mathcal{S}_t(x)$, from each tree $t \in \mathcal{T}$, should be accounted (used) for the final prediction of y. In our proposed approach, the weights are then calculated as

$$w_{tj}(x) = \frac{\mathbb{1}\{X_j \in \mathcal{S}_t(x)\}}{\sum_{n}^{N} \mathbb{1}\{X_n \in \mathcal{S}_t(x)\}}. \tag{2}$$

Note that each tree $t \in \mathcal{T}$ uses different bootstrapped samples from N training observations. Gathering these weights together, it is possible to construct the empirical conditional relative frequency distributions of the response variable, which can then be used for the prediction of different quantiles. The prediction of a single tree can then be computed as

$$\hat{y}_{t,j}(x) = \sum_{j}^{N} w_{tj}(x) Y_j. \tag{3}$$

To use the whole RF, consisting of trees trained on different bootstrapped samples X_j, one can then estimate the expected value of the response as

$$\hat{y}_j(x) = \mathbb{E}(Y \mid X = x) = \sum_{j}^{N} w_j(x) Y_j \tag{4}$$

where

$$w_j(x) = \frac{1}{|\mathcal{T}|} \sum_{t \in \mathcal{T}} w_{tj}(x), \ \forall\, j = 1, 2, \dots, N \tag{5}$$

Then the conditional quantile functions can be estimated for quantile probability levels τ as

$$Q_\tau(x) = \inf\{y : \hat{F}(y \mid X = x) \ge \tau\}. \tag{6}$$

We note that to assess the quality of the developed forecasting models and avoid over-fitting to the training observations, performance metrics shall be calculated based on the out-of-bag (*oob*) samples [37]. During the training procedure with RF, in our coding of the technique, the available data are sampled with replacement, creating bootstrap samples specific to each individual learner of the ensemble. Then, the prediction errors are estimated using the samples that do not belong to the specific bootstrapped samples used for training tree $t \in \mathcal{T}$ (*oob* samples). In this way the *oob* ensemble error estimator is unbiased for the true ensemble error. Therefore, the tuning of the RF parameters can be done based on this, instead of implementing cross-validation.

Finally, we note that our case considers two random response variables, y: the load (power consumption P^{ℓ}) of the platform, and the wind power produced by the wind farm P^{w}. In the following, we thus consider two separate QRF models, one for each of these random variables.

2.2. Model selection and performance

RFs have a low number of hyper-parameters, the main one being the number of trees $|\mathcal{T}|$ that compose the forest. A common data-driven strategy for selecting $|\mathcal{T}|$ is to analyze statistical performance indexes that are commonly used for regression metrics, such as mean squared

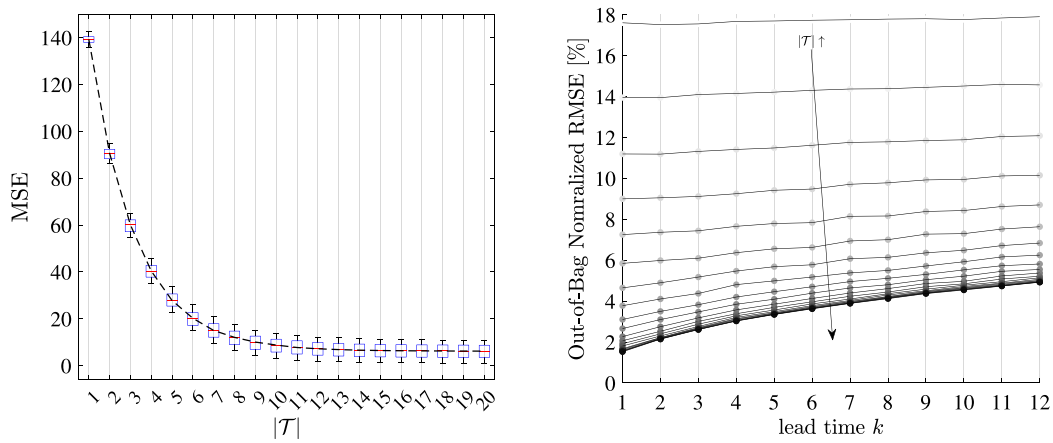

(a) Mean Squared Error (MSE) metric for all lead times and increasing the number of trees in the random forest.

(b) Normalized Root Mean Squared Error (NRMSE) for different numbers of trees in the random forest and increasing lead time.

Fig. 1. Regression model selection based on out-of-bag performance metrics for different lead times and number of trees in the random forest.

error (MSE) and normalized root mean squared error (NRMSE) for the *oob* samples, i.e.,

$$MSE(k) = \frac{1}{\sum_{j=1}^{N} w_{j,k}} \sum_{j=1}^{N} w_{j,k} \left(Y_j(k) - \hat{y}_j(k)\right)^2 \tag{7}$$

and

$$NRMSE(k) = \frac{1}{P_n} \sqrt{\frac{1}{N} \sum_{j=1}^{N} w_{j,k} \left(Y_j(k) - \hat{y}_j(k)\right)^2}. \tag{8}$$

For example, following this approach leads to results for the random variable P^{ℓ} such as in Figs. 1(a) and 1(b). In particular, in Fig. 1(a) we observe that increasing the number of trees inside the forest generally results in decreasing the resulting MSE for all the lead times $k \in \mathcal{K}$. This decrease is bigger and significant for low trees number, and it becomes less significant as the ensemble of trees grows, until it levels off around $|\mathcal{T}| = 20$. A similar trend is noticed in Fig. 1(b), plotting the relation between the number of trees and lead times. This figure shows that, in general, smaller lead times are associated with smaller NRMSE, meaning that (as intuition would say) short-term predictions are better compared to longer-term ones. However, as the number of trees approaches 20, the NRMSE improvement becomes negligible, as we observe from the increased density of the curves at the lower part of the diagram.

Let us note that the scope of this paper is not to improve the QRF method, but rather to demonstrate its applicability and suitability as a good non-linear probabilistic estimator for regression problems with intricate non-linear patterns and how this can be integrated into the optimal energy management, leading to potential benefits (as presented in detail in Section 4).

To demonstrate the performance of the developed forecasting models for each random variable, a reference period was selected and the output of the forecasting results for different lead times was monitored, as illustrated in Fig. 2. As we observe from Fig. 2(a), the one step ahead forecasting model ($k = 1$) can accurately predict the expected value of the true response, despite the step variations (i.e., within 15 min) of the load profile. However, as the lead time increases ($k = 6$), the predictions become less accurate (especially when close to the steps). This demonstrates the challenge of performing precise and detailed prediction of steps for further look ahead times.

We can also note the following interesting behavior of the forecaster: when load profiles tend to be constant, the predictions become more noisy for larger look ahead times, reflecting the deterioration of the forecasts as we look further steps ahead. Similar patterns can also be noticed from Figs. 2(c) and 2(d), where for $k = 1$ the predictions follow accurately the data, while $k = 6$ leads to a remarkably worse quality of the predictions, especially close to the local minima and maxima resulting from wind power ramps-up and ramps-down.

3. Isolated power system modeling and stochastic model predictive controller

This section introduces the model of the system to be controlled, i.e., the isolated power system integrating a wind farm and energy storage. A schematic of the consider system is presented in Fig. 3.

3.1. Control system

The control system under consideration is composed of a continuous state, related to the BESS subsystem and discrete ones (binaries) related to the operational status (on/off) of the Gas Turbines (GTs). The system state can be expressed as

$$\mathbf{x} = \left[x^{SoC}, \mathbf{x}^{gt}_{1:N_g}\right]^T \quad \forall\, g = 1, \dots, N_g \tag{9}$$

where the control input is again hybrid composed of continuous variables (charging and discharging power) and discrete (binary) signals indicating turning on/off of a GT unit. This is expressed as

$$\mathbf{u} = \left[P^{ch}, P^{dis}, b_1^{gt,on}, b_1^{gt,off}, \dots, b_{N_g}^{gt,on}, b_{N_g}^{gt,off}\right]^T \tag{10}$$

Then, given an initial condition

$$\mathbf{x}_0 = \left[x_0^{SoC}, \mathbf{x}^{gt}_{0,1:N_g}\right]^T \tag{11}$$

and an optimal control action at $k = 0$

$$\mathbf{u}_0 = \left[P_0^{ch,*}, P_0^{dis,*}, b_{0,1}^{gt,on,*}, b_{0,1}^{gt,off,*}, \dots, b_{0,N_g}^{gt,on,*}, b_{0,N_g}^{gt,off,*}\right]^T \tag{12}$$

we can express the updated state as

$$\mathbf{x}_+ = \boldsymbol{A}_0 \mathbf{x}_0 + \boldsymbol{B}_0 \mathbf{u}_0 \tag{13}$$

where the system matrices are defined as

$$\boldsymbol{A}_0 = diag\left\{ \mathbb{1}^T_{\{1:|\mathcal{K}|\}} \right\} \tag{14}$$

$$\boldsymbol{B}_0 = \begin{bmatrix} \left[\frac{\eta_{ch} T_s}{60\overline{E}^b}, \frac{\eta_{dis}^{-1} T_s}{60\overline{E}^b}\right] & \mathbf{0}_{1\times N_g} \\ \mathbf{0}_{2\times N_g} & \boldsymbol{G}_0 \end{bmatrix} \tag{15}$$

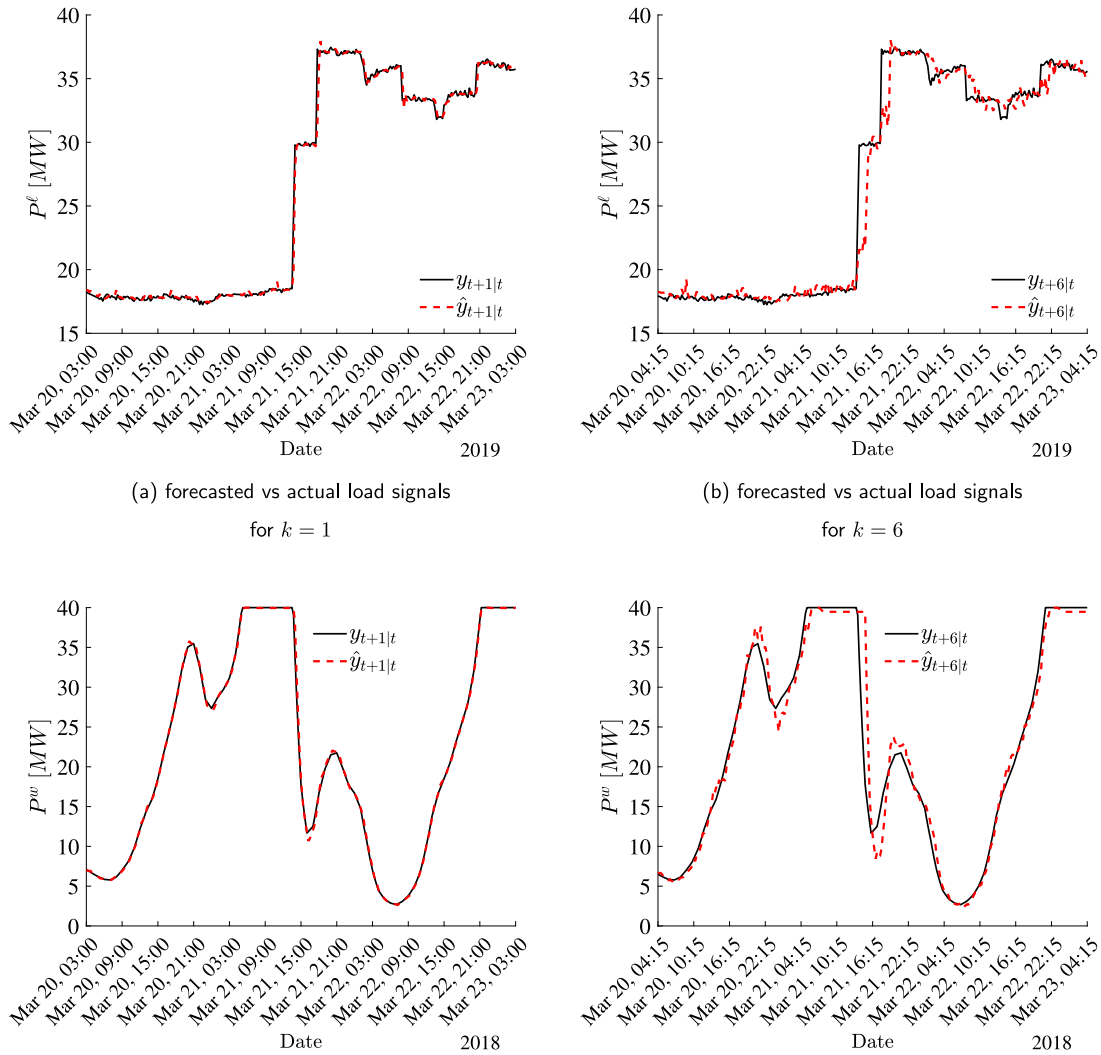

(a) forecasted vs actual load signals for $k = 1$

(b) forecasted vs actual load signals for $k = 6$

(c) forecasted vs actual wind power signals for $k = 1$

(d) forecasted vs actual wind power signals for $k = 6$

Fig. 2. Forecasted (red) vs actual (black) load and wind power signals using the corresponding developed auto-regressive Random Forest models for different prediction horizons ($k = 1,\ k = 6$)

where $\boldsymbol{G}_0$ is a $4\times N_g$ matrix (i.e., the dimensions defined by the number of gas turbines and associated control actions) defined as

$$\boldsymbol{G}_0 = \begin{bmatrix} 1 & -1 & 0 & \cdots & 0 \\ 0 & 0 & \ddots & 0 & 0 \\ 0 & 0 & \cdots & 1 & -1 \end{bmatrix} \tag{16}$$

The setpoints of the gas turbine (GT, continuous) and of the dumping power (continuous), which are outputs of the economic optimal control law, are inputs to the power system but are not considered as part of control system, since they do not affect the state as defined in Eq. (9). Thus, for notational consistency, they are not included in the vector u but they are defined as

$$\mathbf{v} = \left[P_1^{gt}, \ldots, P_{N_g}^{gt}, P^d\right]^T \tag{17}$$

In the following, the control system variables (Eqs. (9), (10) and (17)) are associated with the islanded power grid components, through the modeling of each subsystem's operation.

3.2. Gas turbines operation

To capture the detailed operation of the GT units, the fuel/efficiency curve needs to be accurately modeled. The non-linear curve $\mathcal{F}_{fuel}$ is approximated though Piece-Wise Linear (PWL) functions as in [40] (details in Appendix B). Then $\forall\, k \in \mathcal{K},\ g = 1, \ldots, N_g,\ \omega = 1, \ldots, N_\omega$ we have

$$P_{k,\omega,g}^{gt} = \mathbf{D}_P^{gt\,T}\, \mathbf{w}_{k,\omega,g}^{fuel} \tag{18}$$

$$x_{k,\omega,g}^{gt} - x_{k-1,g}^{gt} \le b_{k,\omega,g}^{gt,on} \tag{19}$$

$$x_{k-1,g}^{gt} - x_{k,\omega,g}^{gt} \le b_{k,\omega,g}^{gt,off} \tag{20}$$

$$x_{k,\omega,g}^{gt} = x_{k-1,\omega,g}^{gt} + b_{k,\omega,g}^{gt,on} - b_{k,\omega,g}^{gt,off} \tag{21}$$

$$b_{k,\omega,g}^{gt,on} + b_{k,\omega,g}^{gt,off} \le 1 \tag{22}$$

$$|\, P_{k,\omega,g}^{gt} - P_{k-1,\omega,g}^{gt} \,| \le 4\frac{T_s}{60} RR \tag{23}$$

$$P_{k,\omega,g}^{gt} \le \overline{P}^{gt}\, x_{k,\omega,g}^{gt} \tag{24}$$

$$\underline{P}^{gt}\, x_{k,\omega,g}^{gt} \le P_{k,\omega,g}^{gt} \tag{25}$$

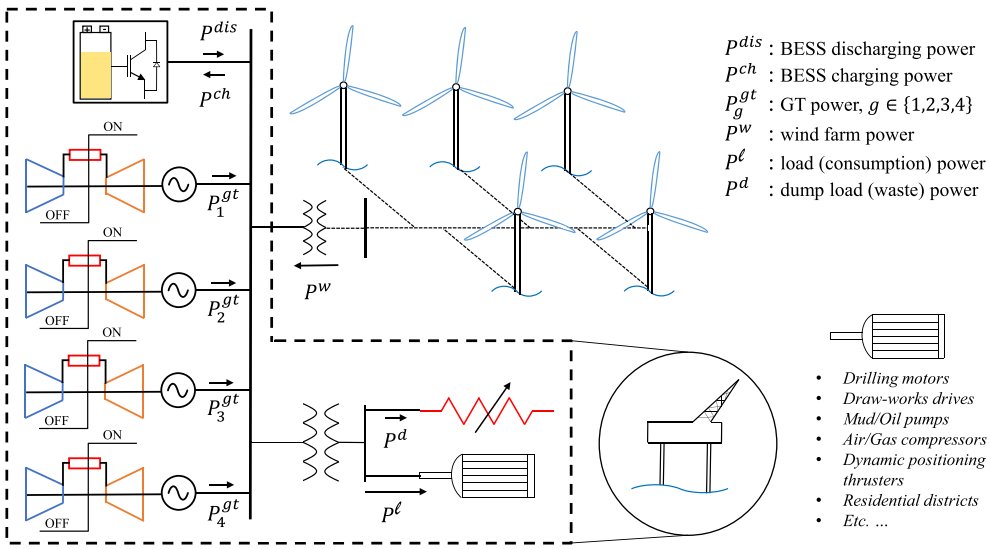

Fig. 3. Simplified single-line diagram of the Oil & Gas installation integrates wind power from a local wind farm, a battery energy storage system, a controllable load for excess energy dumping, and an aggregated load representing the total load to be covered by the power generation systems.

Following [25] we model the common control action at $k = 0$ as

$$P_{0,\omega,g}^{gt} = P_{0,g}^{gt} \quad \forall\, g = 1,\dots,N_g,\ \omega = 1,\dots,N_\omega \tag{26}$$

Note that no additional variables are needed to bind the binary variables $b_{k,\omega}^{gt,on}$ to be the same at $k = 0$, $\forall\ \omega = 1,\dots,N_\omega$ because this is enforced by Eq. (26).

3.3. Battery energy storage system

3.3.1. Dynamics

The charging/discharging power is modeled through the following set of linear equations

$$P_{k,\omega}^{dis} \le \overline{P}^b b_{k,\omega}^{dis} \tag{27}$$

$$P_{k,\omega}^{ch} \le \overline{P}^b (1 - b_{k,\omega}^{dis}) \tag{28}$$

Following again [25], we model the common control action at $k = 0$ as

$$P_{0,\omega}^{ch} = P_0^{ch} \quad \forall\ \omega = 1,\dots,N_\omega \tag{29}$$

$$P_{0,\omega}^{dis} = P_0^{dis} \quad \forall\ \omega = 1,\dots,N_\omega \tag{30}$$

We can then express the charging and discharging variables $\forall\ k \in \mathcal{K},\ \omega = 1,\dots,N_\omega$ in compact form as

$$\mathbf{P}^{dis} = \left[P_{0,1}^{dis},\dots,P_{|\mathcal{K}|,1}^{dis},\dots,P_{0,N_\omega}^{dis},\dots,P_{|\mathcal{K}|,N_\omega}^{dis}\right]^T \tag{31}$$

$$\mathbf{P}^{ch} = \left[P_{0,1}^{ch},\dots,P_{|\mathcal{K}|,1}^{ch},\dots,P_{0,N_\omega}^{ch},\dots,P_{|\mathcal{K}|,N_\omega}^{ch}\right]^T \tag{32}$$

Then the continuous state of the BESS can be expressed as

$$x_{k,\omega}^{SoC} = 1 - DoD_{k,\omega} \tag{33}$$

where $DoD_{k,\omega}$ represents the depth-of-discharge $\forall\ k \in \mathcal{K},\ \omega = 1,\dots,N_\omega$ and given the initial condition $E_0^b = x_0^{SoC}\overline{E}^b$ we can express its time evolution as

$$\begin{aligned}\mathbf{1} - \left(\frac{E_0^b}{\overline{E}^b} diag\left\{\mathbb{1}^T_{\{1:|\mathcal{K}|\times N_\omega\}}\right\} + \frac{T_s}{60\overline{E}^b}\boldsymbol{B}\left(\eta_{ch}\mathbf{P}^{ch} - \eta_{dis}^{-1}\mathbf{P}^{dis}\right)\right)\\ = diag\left\{\mathbb{1}^T_{\{1:|\mathcal{K}|\times N_\omega\}}\right\}\mathbf{DoD}\end{aligned} \tag{34}$$

where

$$\mathbf{DoD} = \left[DoD_{0,1},\dots,DoD_{|\mathcal{K}|,1},\dots,DoD_{0,N_\omega},\dots,DoD_{|\mathcal{K}|,N_\omega}\right]^T \tag{35}$$

subject to

$$\begin{aligned}E_0^b diag\left\{\mathbb{1}^T_{\{1:|\mathcal{K}|\times N_\omega\}}\right\} + \frac{T_s}{60}\boldsymbol{B}\left(\eta_{ch}\mathbf{P}^{ch} - \eta_{dis}^{-1}\mathbf{P}^{dis}\right)\\ \le diag\left\{\mathbb{1}^T_{\{1:|\mathcal{K}|\times N_\omega\}}\right\} SoC_{max}\overline{E}^b\end{aligned} \tag{36}$$

$$\begin{aligned}E_0^b diag\left\{\mathbb{1}^T_{\{1:|\mathcal{K}|\times N_\omega\}}\right\} + \frac{T_s}{60}\boldsymbol{B}\left(\eta_{ch}\mathbf{P}^{ch} - \eta_{dis}^{-1}\mathbf{P}^{dis}\right)\\ \ge diag\left\{\mathbb{1}^T_{\{1:|\mathcal{K}|\times N_\omega\}}\right\} SoC_{min}\overline{E}^b\end{aligned} \tag{37}$$

where $\boldsymbol{B}$ is defined in Appendix B.

3.3.2. Battery degradation

Similarly, following [41] and again using piecewise affine approximations [40] for the curve $\mathcal{F}_{deg}$, the battery degradation can be expressed as a combination of linear equations (details in Appendix B). Then, $\forall\ k \in \mathcal{K},\ \omega = 1,\dots,N_\omega$ we have

$$DoD_{k,\omega} = \mathbf{D}_{dod}^{deg\,T}\mathbf{w}_{k,\omega}^{deg} \tag{38}$$

$$\rho_{k,\omega} = \mathbf{D}_{cyc}^{deg\,T}\mathbf{w}_{k,\omega}^{deg} \tag{39}$$

$$d_{k,\omega} \ge \frac{1}{2}\mid \rho_{k,\omega} - \rho_{k-1,\omega} \mid \tag{40}$$

$$D_\omega^{cyc} \ge \sum_{k\in\mathcal{K}} d_{k,\omega} \quad \forall\ \omega = 1,\dots,N_\omega \tag{41}$$

3.4. Wind turbines

The wind power generation is then modeled after the basic power curve of the reference case wind turbines, i.e., as

$$P_{k,\omega}^w(w_{k,\omega}) = \begin{cases}0, & w_{k,\omega} \le w_{ci}\\ N_w P_n^w\left(\frac{w_{k,\omega}}{w_n}\right)^3, & w_{ci} \le w_{k,\omega} \le w_n\\ N_w P_n^w, & w_n \le w_{k,\omega} < w_{co}\\ 0, & w_{co} \le w_{k,\omega}\end{cases} \tag{42}$$
$$\forall\ k \in \mathcal{K},\ \omega = 1,\dots,N_\omega$$

where w_{ci} is the cut-in wind speed; w_n is the nominal wind speed; w_{co} is the cut-off wind speed; P_w^n is the nominal power of each wind turbine; and N_w is the number of wind turbines in the considered wind farm.

3.5. Stochastic model predictive controller design

Then, by interconnecting the control system with its sub-components, as defined in Sections 3.1–3.3 and 3.3.2 with the power system including the stochastic disturbance as described below, we can formulate the proposed Stochastic Model Predictive Controller (SMPC).

3.5.1. Power system

The grid dynamics are expressed through the power balance as

$$\sum_{g}^{N_g} P^{gt}_{k,\omega,g} = P^{ch}_{k,\omega} - P^{dis}_{k,\omega} + P^{d}_{k,\omega} + \xi_{k,\omega} \quad \forall\, k \in \mathcal{K},\ \omega = 1,\dots,N_\omega \tag{43}$$

where $\xi_{k,\omega}$ is the random disturbance composed of load and wind power values at lead time k, formed by scenarios $\omega = 1,\dots,N_\omega$, as described in Section 3.5.2. By iteratively evaluating Eq. (13) we can then forecast the trajectory $\mathbf{X}_+ = \left[\mathbf{x}_{t+0|t},\dots,\mathbf{x}_{t+k|t},\dots,\mathbf{x}_{t+|\mathcal{K}||t}\right]^T$ for the BESS and GT states that are associated with a particular realization ω of the random disturbance signal $\boldsymbol{\xi}_\omega = \left[\xi_{1,\omega},\dots,\xi_{|\mathcal{K}|,\omega}\right]^T$ (see Eq. (48)).

3.5.2. Scenario generation

We now describe a statistically motivated data-driven strategy for generating the scenarios that shall then be used within the stochastic control strategy proposed by this paper.

To arrive at the formulation of the scenarios generation mechanism, we start then by assuming that the predictive QRF models for the random variables P^p, with $p = \{\ell, w\}$, have been estimated as proposed in Section 2. We then note that by using Probability Inverse Transforms, Cholseky decompositions [25,42], and Gaussian copulas [43], it is possible to generate scenarios and populate the random disturbance signals $\boldsymbol{\xi}_\omega$ as follows: for each random variable (i.e., both wind and load power), we can get the quantile function (inverse CDF) by interpolating among the set of pre-calculated quantile values as

$$\hat{F}^{p\,-1}_{t+k|t}\left(P^p_{t+k} \mid \left[P^p_t, P^p_{t-1},\dots,P^p_{t-L}\right]\right) = \left\{Q^p_{\tau,k}\left(\left[P^p_t, P^p_{t-1},\dots,P^p_{t-L}\right]\right)\right\}_{\tau\in[0,1]} \quad \forall\, k \in \mathcal{K}. \tag{44}$$

Then, by applying the empirical CDF to the quantile function, we get a new random variable U^p_{t+k} uniformly distributed and then by using the inverse Gaussian CDF, we can generate random variables that are normally distributed as

$$\mathcal{X}^p_{t+k} = \Phi^{-1}(U^p_{t+k})\ \forall\, k \in \mathcal{K}. \tag{45}$$

Defining $\mathcal{X}^p_t = \left\{\mathcal{X}^p_{t+k}\right\}_{k\in\mathcal{K}}$ as a vectorized random variable, we can calculate its empirical covariance for each time step t in an adaptive and recursive way as in [42] by means of

$$\Sigma^p_t = \mu\Sigma^p_{t-1} + (1-\mu)\mathcal{X}^p_t\mathcal{X}^{p\,T}_t, \tag{46}$$

where μ is the forgetting factor of the exponential forgetting scheme, as in [42]. Then, the empirical co-variance can be scaled to get the corresponding correlation matrix R^p_t from which, using a standard normal $\mathbf{z} \sim \mathcal{N}(0,1)$ and the Cholesky decomposition $R^p_t = P^p_t P^{p\,T}_t$, it is possible to generate normal random variables, correlated as in R^p_t, by $\mathbf{z}_c = \mathbf{z}P^p_t$. Finally, by using the Gaussian copula technique, we can generate correlated samples of the random variables P^p as

$$\mathcal{Y}^p = \hat{F}^{p\,-1}_{t+k|t}\left(\Phi(\mathbf{z}_c)\right),\ \forall\, k \in \mathcal{K}. \tag{47}$$

where $\mathcal{Y}^p = \left\{y^p_{t+k|t}\right\}_{k\in\mathcal{K}}$ and $y^p_{t+k|t} \sim \hat{F}^p_{t+k|t}$. In this way we can generate auto-correlated realizations (scenarios)

$$\xi_{k,\omega} = y^{\ell,(\omega)}_{t+k|t}\, s_r - y^{w,(\omega)}_{t+k|t} \quad \forall\, k \in \mathcal{K},\ \omega = 1,\dots,N_\omega \tag{48}$$

where s_r is the spinning reserve (percentage). Such scenarios will then be used in the stochastic optimization problem defined below.

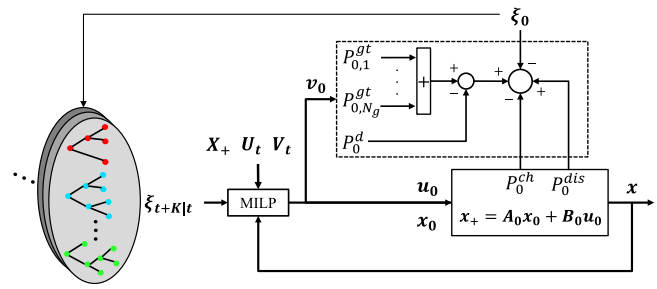

Fig. 4. Control schematic.

3.5.3. Objective function

To formulate an optimization problem, one must also define the objective function, that in our case will correspond to an optimal control law whose decision variables are $\mathbf{U}^*_\mathbf{t} = \left[\mathbf{u}_{t+0|t},\dots,\mathbf{u}_{t+k|t},\dots,\mathbf{u}_{t+|\mathcal{K}||t}\right]^T$ and $\mathbf{V}^*_\mathbf{t} = \left[\mathbf{v}_{t+0|t},\dots,\mathbf{v}_{t+k|t},\dots,\mathbf{v}_{t+|\mathcal{K}||t}\right]^T$ for any given time step t, where $\mathbf{V_t}$ is the vector of additional optimization variables not considered as inputs to the control system as defined in Eq. (17) (i.e., GT setpoints and dumping power). More precisely, we consider an optimization problem corresponding to the economic SMPC

$$\begin{aligned}
&\text{SP:}\quad \min_{\mathbf{U_t},\mathbf{V_t}} \left\{\mathbb{E}_\omega\left[f(\mathbf{X}_+;\mathbf{U_t};\mathbf{V_t};\boldsymbol{\xi}_\omega)\right]\right\}\\
&\text{where,}\quad f\left(\mathbf{X}_+;\mathbf{U_t};\mathbf{V_t};\boldsymbol{\xi}_\omega\right) = C^{fuel}_\omega + C^{gt,str}_\omega + C^{gt,on}_\omega + C^{deg}_\omega + C^{d}_\omega\\
&\text{s.t.}\quad \boldsymbol{K}\mathbf{X}_+ + \boldsymbol{L}\mathbf{U_t} + \boldsymbol{M}\mathbf{V_t} + \boldsymbol{N}\boldsymbol{\xi}_\omega \preceq \mathbf{0},\\
&\qquad \boldsymbol{K}_{eq}\mathbf{X}_+ + \boldsymbol{L}_{eq}\mathbf{U_t} + \boldsymbol{M}_{eq}\mathbf{V_t} + \boldsymbol{N}_{eq}\boldsymbol{\xi}_\omega = \mathbf{0},\quad \forall\, \omega = 1,\dots,N_\omega.
\end{aligned} \tag{49}$$

where $\boldsymbol{K},\boldsymbol{L},\boldsymbol{M},\boldsymbol{N},\boldsymbol{K}_{eq},\boldsymbol{L}_{eq},\boldsymbol{M}_{eq},\boldsymbol{N}_{eq}$ are matrices of appropriate size expressing the linear constraints Eqs. (13)–(43), and the terms of the cost functions are defined as

$$C^{fuel}_\omega = \frac{T_s}{60}c_f \sum_{k\in\mathcal{K}}\sum_{g\in N_g} \mathbf{D}^{gt\,T}_f \mathbf{w}^{fuel}_{k,\omega,g} \tag{50}$$

$$C^{gt,str}_\omega = c^{str}_{gt} \sum_{k\in\mathcal{K}}\sum_{g\in N_g} b^{gt,on}_{k,\omega,g} \tag{51}$$

$$C^{gt,on}_\omega = \frac{T_s}{60}c^{on}_{gt} \sum_{k\in\mathcal{K}}\sum_{g\in N_g} x^{gt}_{k,\omega,g} \tag{52}$$

$$C^{deg}_\omega = \left(c_{b,rpl} - c_{b,res}\right) D^{cyc}_\omega \tag{53}$$

$$C^{d}_\omega = \frac{T_s}{60}c_d \sum_{k\in\mathcal{K}} P^d_{k,\omega}. \tag{54}$$

We note that the cost function defined in Eq. (49) can be numerically approximated using Sample Average Approximations (SAA) and equiprobable scenarios issued by the developed probabilistic forecasting model described in Section 2. Considering the real time applicability of the proposed method and the solution time of the stochastic optimization problem at each time step, the number of scenarios was set equal to 10. Under the lack of generalized theoretical instructions for the exact number of scenarios to be used in the non-convex MILP optimization problems, this number was selected as a trade-off among practical implementation, computational complexity, and solution quality (tight termination criteria for branch-and-cut methods).

Under the proposed framework, the optimal control action $\mathbf{u}_0$ to be applied at time step t is found as $\mathbf{u}_0 = \mathbf{U}^*_{\mathbf{t},\mathbf{1}}$. Correspondingly, the state of the system is updated through Eq. (13), and the optimal setpoints of the GT and dumped power are given by $\mathbf{v}_0 = \mathbf{V}^*_{\mathbf{t},\mathbf{1}}$. The control schematic diagram is illustrated in Fig. 4.

4. Simulation results and analysis

This section assesses the potential benefits of applying the proposed methodology to the case of an isolated wind-powered O&G

platform with energy storage, against a deterministic MPC strategy counterpart. The approach is thus first investigating the performance of the integrated forecasting algorithm proposed in Section 2, and then comparing the control performance of the proposed SMPC EMS against its deterministic counterpart.

To make such comparisons realistic and valuable, actual load measurements were used from the available datasets (with 15 min time resolution), while the wind power generation data were derived from hourly wind speed timeseries data, publicly available at [44,45] for the specific offshore location of the platform. These measurements were linearly interpolated to match the load timeseries resolution (15 min), allowing for the use of a $T_s = 15$ minutes simulation timestep for the rest of the considered components as well (i.e., battery storage and gas turbines).

4.1. Assessing the capability of the scenario generation mechanism in capturing irregular events

The proposed stochastic control scheme cannot be effective if its integrated forecasting capability is not effective. To assess this last effectiveness, the performance of the forecaster is here assessed based on commonly used metrics first, and then also by examining specific cases of particularly interesting irregular events.

4.1.1. Continuously ranked probability score

Since the QRF model developed in Section 2.1 is used to perform probabilistic forecasting, we assess its performance based on the commonly used metric of Continuously Ranked Probability Score (CRPS) [25,46,47] and by comparing it against a benchmark method. Respectively, this score is defined as a function of k, for an observation y_{t+k} of the random response variable Y_{t+k} with empirical CDF $\hat{F}_{t+k|t}(y) = \mathbf{P}\left[Y_{t+k} \leq y\right]$ as

$$CRPS(\hat{F}_{t+k|t}, y_{t+k}) = \int_{supp(Y_{t+k})} \left(\hat{F}_{t+k|t}(y) - \mathbb{1}\{y_{t+k} \leq y\}\right)^2 dy \tag{55}$$

and is numerically calculated for a test time period $t \in T_{test}$ as

$$CRPS(t,k) = \sum_{\underline{y}_{t+k}}^{y_{t+k}} \hat{F}^2_{t+k|t}(y)dy + \sum_{y_{t+k}}^{\overline{y}_{t+k}} \left(\hat{F}_{t+k|t}(y) - 1\right)^2 dy \tag{56}$$

where $supp(Y_{t+k}) = [\underline{y}_{t+k}, \overline{y}_{t+k}]$ is the support of random variable Y_{t+k} and dy a fine discretization of the values that the random variable can take, given its support.

As for the benchmark algorithm, we perform comparisons against the method from [48], named *CH-PeEn*, which to our knowledge is often used as a universal benchmarking method for a fair comparison. This method basically uses the whole historical dataset to construct distributions of the random variables first, and then uses this information to produce probabilistic forecasts. Note that we constructed a separate model for each lead time $k \in \mathcal{K}$; its CRPS was then calculated as in Eq. (56), and then compared against the one produced by the *QRF* method for the selected test period ($t \in T_{crps}$, which was set equal to a whole month, i.e., September).

From Fig. 5 we can observe the results of the comparison in a dimensionless form, i.e., after the power values of each variable were rescaled to $[0, 1]$. As it is evident from Fig. 5(a), the proposed *QRF* models, as applied to their corresponding random variable (load/wind power), not only improve significantly the probabilistic forecasts compared to *CH-PeEn*, but also achieve very low CRPS values for all the lead times, with the values becoming slightly worse as the lead time increases. From Fig. 5(b) we observe again the superiority of the *QRF* method over *CH-PeEn* (which, actually, is characterized by particularly high values). This means that the distributions produced by the proposed model are much closer to the observations and less spread around it. Finally, the overall relative improvement for the average CRPS across the lead times and for the models concerning the two random variables (load and wind power), is presented in terms of the skill score [25,46], defined as

$$Sk_{sc} = 1 - \frac{\sum_{t \in T_{test}} \sum_{k \in \mathcal{K}} CRPS_{QRF}(t,k)}{\sum_{t \in T_{test}} \sum_{k \in \mathcal{K}} CRPS_{CH-PeEn}(t,k)}. \tag{57}$$

The numerical results are then presented in Table 1.

Table 1
Skill score improvement.

	$\overline{CRPS}$ [%]	
	P^{ℓ}	P^{w}
CH-PeEn	11.56	22.80
QRF	0.98	2.17
Sk_{sc} [%]	91.51	90.50

4.1.2. Assessing the capability of capturing irregular events

Typical demanding situations for the efficient operation of isolated grids that are dominated by intermittent power supply and rapidly varying loads, are those that are characterized by non-smooth and/or sudden net load trend variations (irregular events). This means that we need to assess the performance of the proposed forecasting model in capturing irregular events, since capturing them means enabling the proposed SMPC counteracting them, ensuring efficient grid operation. Such events can then be generated using the proposed copula method. For the load profiles, step variations were considered as a test case, while for the wind power, specific points of curvature reversal or saturation were selected. Curvature variations can happen in cases where the trend is reversed, so a wind ramp-down is followed by a wind-ramp-up and vice versa. The saturation occurs when the wind farm reaches its nominal power production capacity.

In Fig. 6 we see the results of the forecasting capabilities of the proposed approach for different characteristic load patterns. In these diagrams we observe both the true data (black line), the expected forecast (mean prediction — dashed red line), prediction intervals at various percentiles (green areas), and also the generated scenarios from the proposed method (dashed purple lines). As we observe, the proposed approach is capable to quantify the uncertainty around a forecast by increasing or decreasing the width of the prediction intervals. In particular, from Fig. 6(a) we see that when there is low uncertainty and the forecasted profile pattern is quite simple (almost constant), this is followed by a set of generated scenarios where all these scenarios follow the same trend. However, when we are heading towards a load step instant, the uncertainty becomes larger and the prediction intervals more spread (Figs. 6(b) and 6(c)). As a result, the anticipated step variation is included in the prediction intervals and as a result, there are scenarios that actually resemble the true variation. This is an important feature, since these scenarios will provide the SMPC information about the existence of possible alternatives for the possible future load patterns. In this way, we get around the inertia problem that characterizes the deterministic forecast, i.e., the tendency for forecasters in the literature to produce patterns that are too similar to the previous values, and do not anticipate deviations. The same is illustrated in Fig. 6(d) for a step decrease in load where we can see that scenarios very close to the actual step can be generated.

Similar results can be noted from Figs. 7 and 8. In particular, from Fig. 7 we see how the uncertainty interval automatically adapts to the time instant of the issued forecasts. This means that it can understand when a change in the signal shape (wind power profile) is happening. Starting with Fig. 7(a), we already observe how the mean forecast (red dashed line) is much affected by the previous values and is not close to the actual curvature. Nevertheless, scenarios very close to the actual shape can be generated. Then, as time moves forward, as we observe from Figs. 7(b)–7(d), the uncertainty interval constantly becomes larger

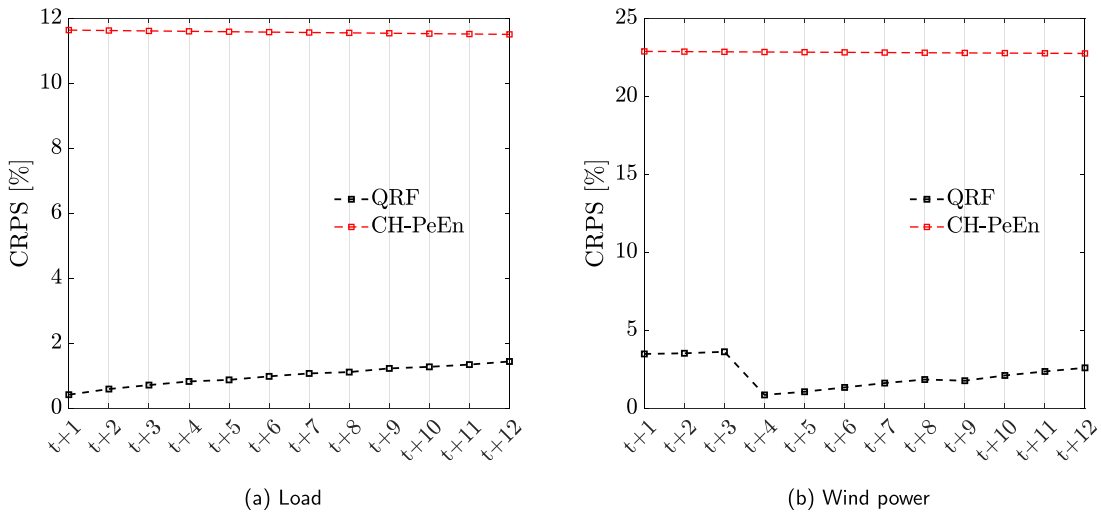

Fig. 5. CRPS for September.

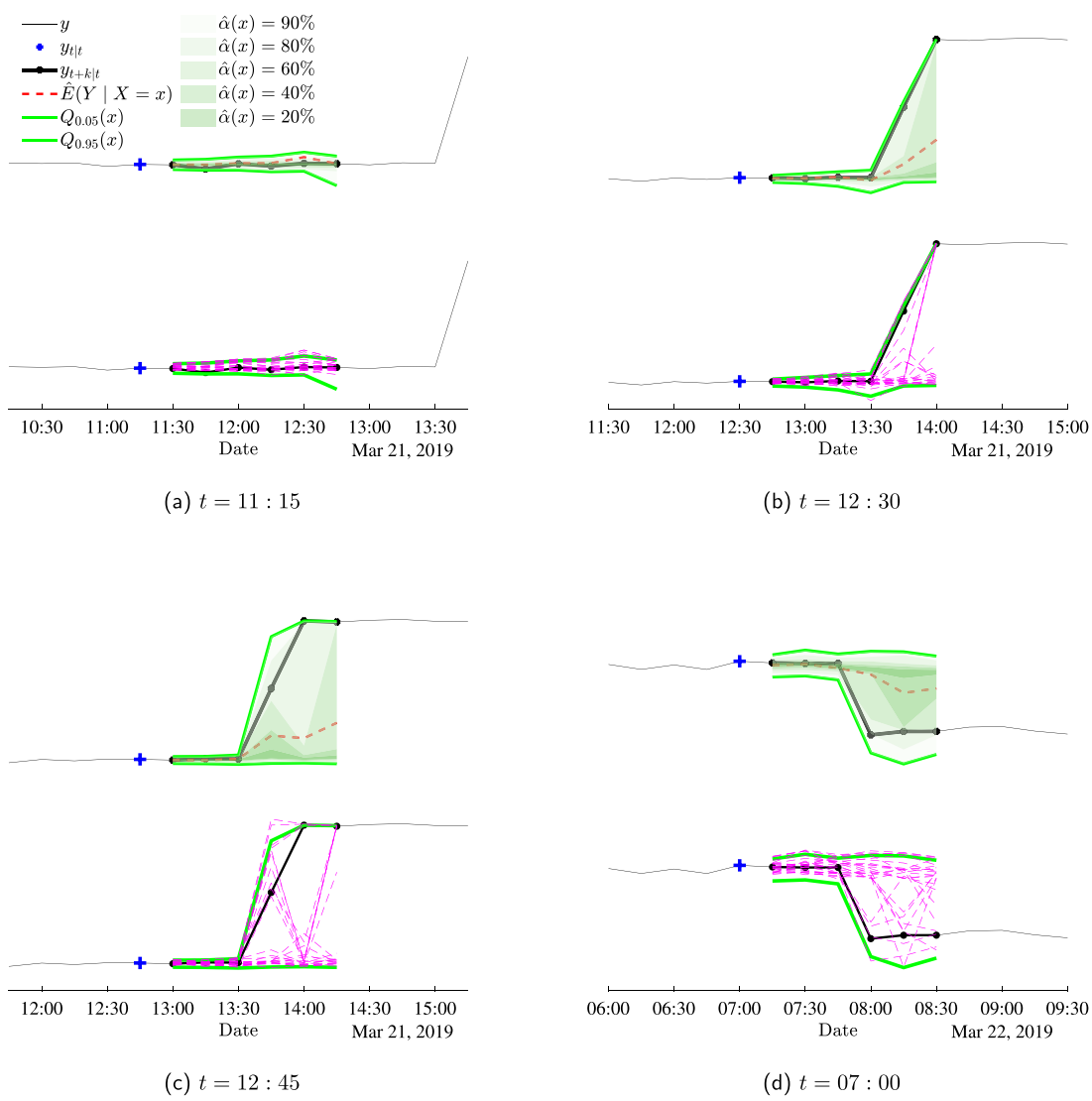

Fig. 6. Various types of an O&G platform's load patterns, reflecting both normal operation and irregular events, such as step variations in both directions. (a) Normal operation (constant loading conditions) (b) Sudden load increase in the near future. Scenarios that accurately capture the variation gradient are generated through the updated (increased) uncertainty interval (c) Moving closer towards the sudden upwards load variation, the updated scenarios closely resemble the shape of the forthcoming load step (d) An example of similar sudden variation, where the load is step-like decreased and the generated scenarios capture this event.

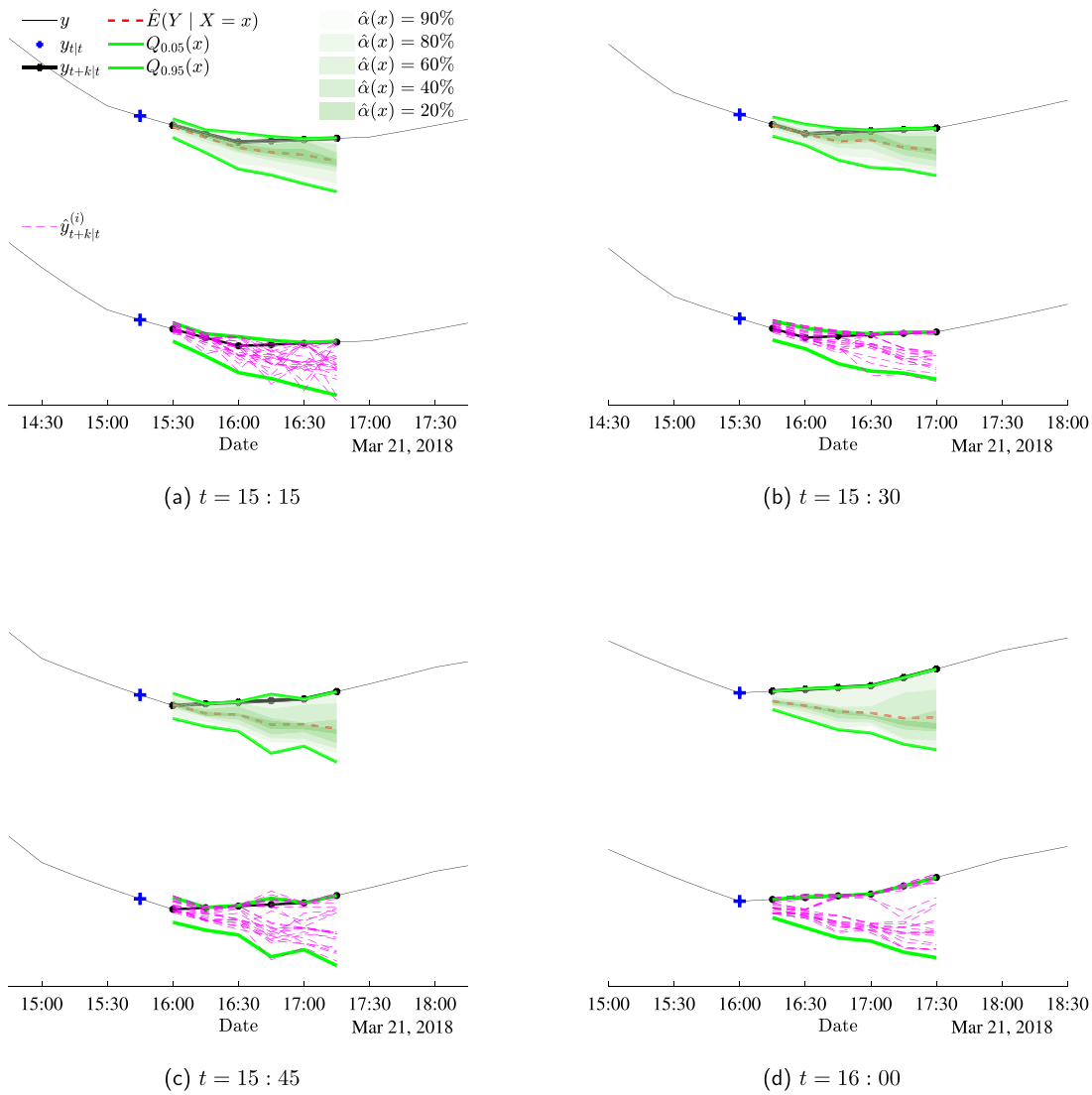

Fig. 7. Example of a trend reversal situation for wind power on 21 March, 15:00–18:00 and successive probabilistic forecasts. Following the sub-figures from top to bottom, we see the updated uncertainty intervals associated with each forecast issue time and the generated scenarios that are able to capture the sudden change from a wind power ramp-down to a ramp-up.

to include the abrupt curvature change and as a result, even when this change is big enough (Fig. 7(d)), scenarios close to reality can be generated. The same characteristics are illustrated in Fig. 8 for a case where the wind power reaches the saturation level.

4.2. Stochastic MPC (SMPC) for energy management under irregular events

We then move to assessing the ensemble of the proposed strategies, i.e., the performance of the integration of the forecasting models developed in Section 2.1 with the proposed MPC formulation described in Section 3.5. The assessment of the proposed method (SMPC) was realized by comparing it against the performance of its deterministic MPC version (DMPC), through numerical simulations. In addition, a benchmark rule-based method was included in the results to better demonstrate/illustrate the effectiveness of the MPC framework for the EMS.

It is noteworthy that the datasets related to our specialized power system application (offshore O&G platform with wind power integration) are characterized by a significant variety of patterns, resulting in different net load profiles. Therefore, to (correctly) assess the proposed method and compare it against other alternatives while capturing the main characteristics of our datasets, different combinations of platform load and wind power generation were considered as case studies. Nevertheless, testing the whole available dataset is computationally intractable, given the restriction of the computational resources and the solution time of the MILP problem on a rolling horizon basis. In this study, the optimization problems were modeled in *Matlab R2020* and solved with *Gurobi 9.1.0* in a 28 physical core multi-node cluster with Intel(R) Xeon(R) CPU E5-2690 v4 @ 2.60 Hz, 25 GB RAM.

However, for the purpose of assessing our method and investigating the potential benefits, some representative daily net load patterns were identified and selected as case studies. They describe typical behaviors present throughout the whole datasets (both load and wind power), capturing in detail the irregular events that are the main target for our method. Such irregular events include sudden transitions from lower to higher loading conditions resembling step-like perturbations that demand the startup or shutdown of an extra GT unit, wind power trend reversals from lower average values ramping up to higher ones and vice versa, or even net load conditions where the operating GT units are marginal, and several switching actions would be required for relatively small net load variation. Capturing case studies with these characteristics allows us to make a more accurate assessment of the

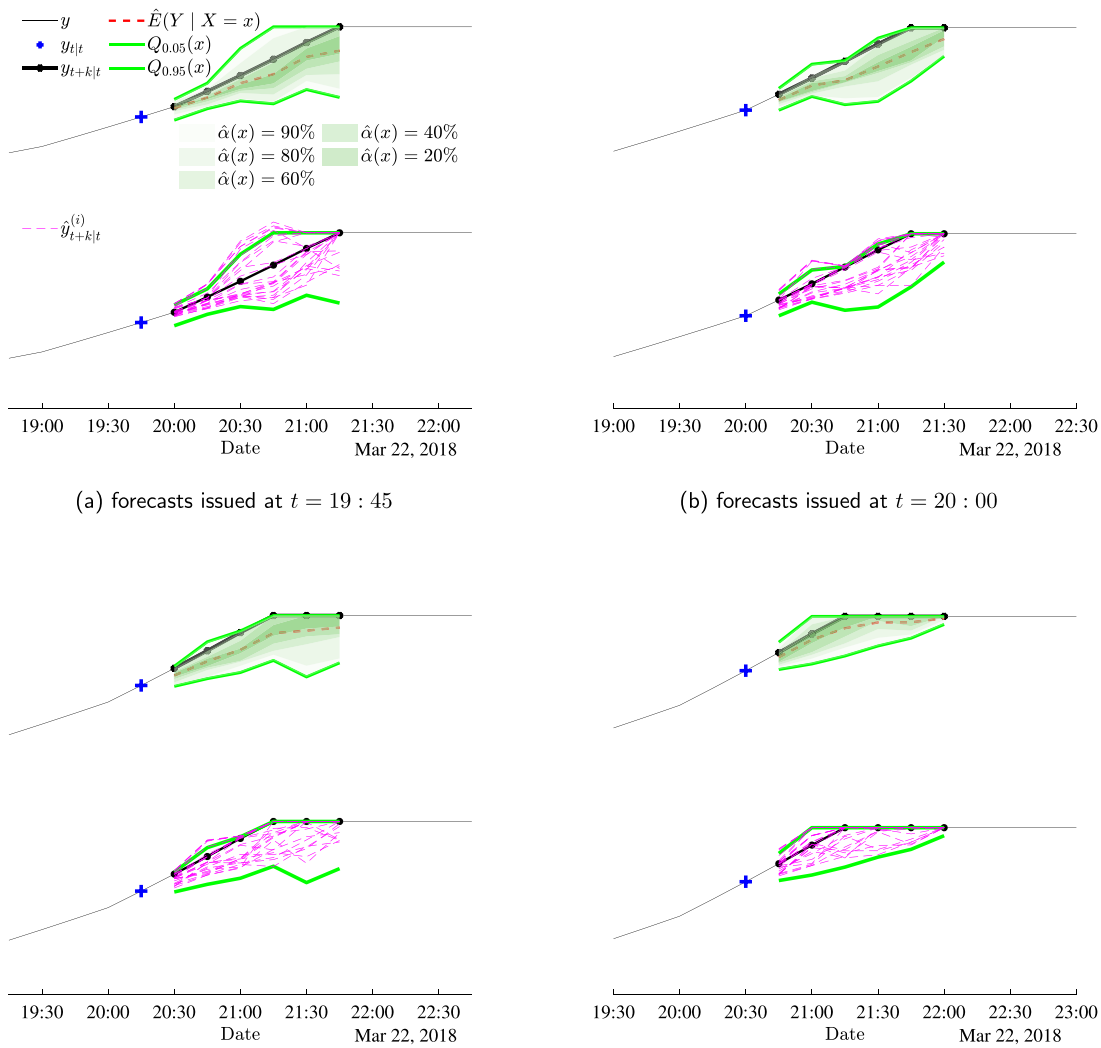

(a) forecasts issued at $t = 19:45$

(b) forecasts issued at $t = 20:00$

(c) forecasts issued at $t = 20:15$

(d) forecasts issued at $t = 20:30$

Fig. 8. Example of a wind power saturation situation on 22 March, 19:00–22:00 and successive probabilistic forecasts. Following the sub-figures from top to bottom, we see how the updated uncertainty intervals associated with each forecast issue time, keep on narrowing down, identifying a saturation event.

proposed method and its applicability to the target applications. The following basic patterns were then considered as case studies.

1. ***LL-SU-WD***: *low* loading conditions including load step *up* under wind ramping *down*
2. ***ML-SD-WU***: *medium* loading conditions including load step *down* under wind ramping *up*
3. ***HL-SUD-WU***: *high* loading conditions including load steps *up and down* and wind ramping *up*
4. ***LL-SDU-WU***: *low* loading conditions including load steps *down and up* and wind ramping up
5. ***HL-SDU-WD***: *high* loading conditions including load steps *down and up* and wind ramping *down*
6. ***HL-WD***: *high* loading conditions (almost steady) and wind ramping *down*

Those cases span different operational regimes such as low (L), medium (M), or high (H) loading (L) conditions relative to the total aggregated platform load, capture different types of irregular events such as load steps up (SU), load steps down (SD), or both in any order (SUD, SDU), and also include the effects of wind power ramping up (WU) and down (WD). To assess the performance and compare the proposed controller ("SMPC") with the deterministic ("DMPC") version, numerical simulations were performed for the above test periods with duration T_t per case. The methods were evaluated and compared in terms of the key performance indices (KPIs) defined in Eqs. (58)–(62). Those reflect the cumulative costs (Eq. (59)) and emissions production (Eq. (58)) from the platform operation, the amount of curtailed energy (Eq. (61)), and the lifetime degradation of the controllable components. The latter can be expressed by the cycling behavior for the BESS (Eq. (62)) and the number of switching signals (on/off) for the GTs (Eq. (60)).

$$I_f(\mathbf{x}_+(t), \mathbf{v}_0(t)) = \frac{T_s}{60} \sum_{t \in T_t} \sum_{g \in N_g} \mathcal{F}_{fuel}(P^{gt}_{0,g}(t)) P^{gt}_{0,g}(t) + c^{idle}_f x^{gt}_{0,g}(t) \tag{58}$$

$$I_c(\mathbf{x}_+(t), \mathbf{u}_0(t), \mathbf{v}_0(t)) = I_f(\mathbf{x}_+(t), \mathbf{v}_0(t)) c_f + c^{str}_{gt} \sum_{t \in T_t} \sum_{g \in N_g} b^{gt,on}_{0,g}(t) \tag{59}$$

$$I_{sw}(\mathbf{u}_0(t)) = \sum_{t \in T_t} \sum_{g \in N_g} b^{gt,on}_{0,g}(t) + \sum_{t \in T_t} \sum_{g \in N_g} b^{gt,off}_{0,g}(t) \tag{60}$$

$$I_{de}(\mathbf{u}_0(t), \mathbf{v}_0(t)) = \frac{T_s}{60} \sum_{t \in T_t} \sum_{g \in N_g} P^{gt}_{0,g}(t) - \left(P^{ch}_0(t) - P^{dis}_0(t)\right) - \xi_0(t) \tag{61}$$

$$I_{dg}(\mathbf{x}_+(t), \mathbf{u}_0(t)) = \sum_{t \in T_t} D^{cyc}(t) \tag{62}$$

where I_f is the total fuel consumption (which can be directly associated with CO_2 emissions because of the linear dependency on the combustion reaction), I_c represents the operational expenditure resulting from the indicated operation of the GTs, I_{sw} accounts for the switching signals turning on or shutting down the GTs expressing the binary control actions, I_{de} is the amount of the actual dumped energy (including the shifted load because of the spinning reserve and safety requirement), and I_{dg} represents the degradation of the BESS as a consequence of the cycling induced by the control action. Those indices encapsulate the effects of the EMS on the operation of the power system under consideration and reflect both economic and environmental aspects.

4.2.1. Case studies assessment

For the analysis of the case studies, we employ the following procedure. First, the actual load, wind power, and resulting net load profiles are plotted together. Net load represents the sequence of values of the disturbance $\xi_0(t),\ \forall\ t = 0, \dots, T_t$ that acts on the platform power system and needs to be estimated by the proposed forecasting method (Section 3.5.2). Then, different colored areas are used on the same plots to indicate different ranges of the values $\xi_0(t)$. These areas highlight the different numbers of operating (turned ON) GTs that would be required to cover the corresponding net load value $\xi_0(t)$ under the following simple benchmark rule-based strategy

if $\xi_0(t) \le 0$ **then**
  $\mathbf{x}^{gt}_{1:N_g}(t) = 0$
else if $\xi_0(t) \le P^{gt}_n$ **then**
  $\mathbf{x}^{gt}_1(t) = 1 \wedge \mathbf{x}^{gt}_{2:N_g}(t) = 0$
else if $\xi_0(t) \le 2P^{gt}_n$ **then**
  $\mathbf{x}^{gt}_{1:2}(t) = 1 \wedge \mathbf{x}^{gt}_{3:N_g}(t) = 0$
else if $\xi_0(t) \le 3P^{gt}_n$ **then**
  $\mathbf{x}^{gt}_{1:3}(t) = 1 \wedge \mathbf{x}^{gt}_{4:N_g}(t) = 0$
else
  $\mathbf{x}^{gt}_{1:N_g}(t) = 1$
end if

In addition, in the same plot on the right axis we can identify the number of on GTs with each proposed method (DMPC/SMPC) and, in this way, we can compare the number of GTs that would be required by each method. This is expressed as

$$I^{gt}_{on}(\mathbf{x}_+(t)) = \sum_{g \in N_g} x^{gt}_g(t) \tag{63}$$

Then, the resulting state of charge trajectories with the DMPC and SMPC methods are plotted together with the common disturbance signal on separate figures and finally, the KPIs defined in Eqs. (58)–(62) are calculated.

4.2.2. Case: LL-SU-WD

First, a case of low loading conditions with a load step up and wind ramp down is demonstrated (Fig. 9). As can be noticed from Fig. 9(a), the load step and the low wind power generation cause the net load to change regime and based on the rule-based strategy, 2 GTs would be required to operate. However, we see from the same figure that under both control algorithms, DMPC and SMPC, after the step, there are some instants where the platform could operate with just a single GT, obtaining the rest energy from the BESS. This is also illustrated in Fig. 9(b) from the SoC trajectories. Initially and up to the load step, both DMPC and SMPC would result in a similar behavior, with the BESS reaching its maximum SoC while charging to provide higher efficiency operating point for the GT. After the step though, the available capacity of the BESS is being used (again by both methods), discharging the battery and providing some extra time for the 1 GT operational regime. From the same figure we also see that at the moment of the step, the proposed SMPC makes better use of the BESS, providing a deeper discharge and thus some extra time to the 1GT regime. Then, some oscillations are induced by both methods while trying to minimize the number of on GTs but also operating them as efficiently as possible not to significantly increase the emissions level. Of course, this behavior increases the BESS degradation, but it highly depends on the weighting of the corresponding cost term (Eq. (53)), in the objective function (Eq. (49)) which in our case was set based on the investment and residual costs of the battery (see Table 9) as in [41]. Different values for the weight would induce different behaviors with possibly fewer oscillations. As the effect of the net load transient vanishes, the SoC trajectories become more similar and converge approaching the end of the day. The improved performance of the SMPC during the (unavoidable) oscillatory behavior is reflected in the fewer GT switching signals (Table 2), avoiding startup costs and eventually resulting in reduced cost at the expense of a slightly higher BESS degradation. In addition, despite these benefits, the proposed SMPC does not significantly deteriorate the energy dumping and the fuel consumption (Table 2).

Table 2
LL-SU-WD KPIs.

KPI	MPC Method		Net
	Mean	*Scn*	
I_c [€]	54,277	51,922	2,354
I_f [tn]	143.53	145.69	−0.266
I_{sw} [–]	17	13	4
I_{de} [MWh]	24.05	24.09	−0.049
I_{dg} [%]	0.311	0.387	−0.076

Table 3
ML-SD-WU KPIs.

KPI	MPC Method		Net
	Mean	*Scn*	
I_c [€]	71,154	66,105	5,049
I_f [tn]	185.74	181.04	4.693
I_{sw} [–]	25	19	6
I_{deg} [MWh]	34.55	34.50	0.051
I_{dg} [%]	0.347	0.452	−0.105

4.2.3. Case: ML-SD-WU

Next, a case with medium loading conditions, a load step down, and a wind power ramp up is presented (Fig. 10). In this case, although a clear step down is observed on the load (early times), after that it is still highly variable alternating between the regimes of 1 and 2 on GTs (Fig. 10(a)). Again, we notice that under the optimal policies of both MPC controllers, we decrease the number of operating GT compared to the rule-based strategy. Even though DMPC and SMPC result in similar SoC trajectories initially, at the first load upwards rise right after the step down, the SMPC realizes that it can operate with a single GT for a bit longer and thus discharges the BESS to provide the additional energy (Fig. 10(b)). After this event, the trajectories deviate but both follow similar trends. In this case, the superiority of the proposed control scheme resulted in significant cost savings coming from both fuel consumption reduction and much fewer GT startups again at the small cost of marginally higher BESS degradation (Table 3).

4.2.4. Case: HL-SUD-WU

Then, an interesting case of high loading conditions with both up and down steps and low to medium wind conditions is examined (Fig. 11). This represents a case where all GTs would be required to provide the necessary power (Fig. 11(a)). As the capacity of the systems is close to its limits (more GTs required), the potential benefits decrease since the flexibility provided by the BESS depends on its (limited) size and how this compares with the power capability of a single GT unit. However, again in this case, the SMPC demonstrated its capability to reduce costs by properly controlling the timing and number of on/off commands to the GTs. As we can see in Fig. 11(b), interestingly the

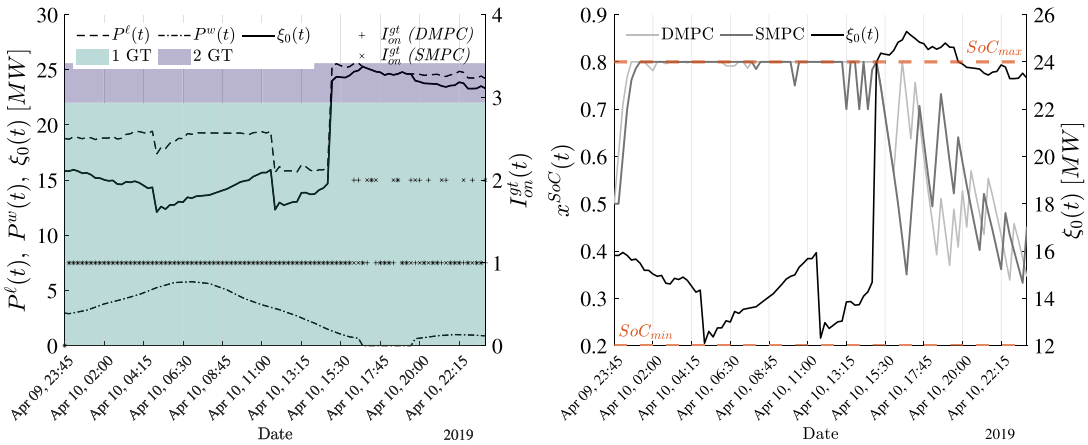

(a) Load, wind power, and net load patterns vs number of on GTs

(b) Net load pattern vs state of charge evolution

Fig. 9. Disturbance and optimal states trajectories (discrete and continuous) with DMPC and SMPC controllers, for the case LL-SU-WD.

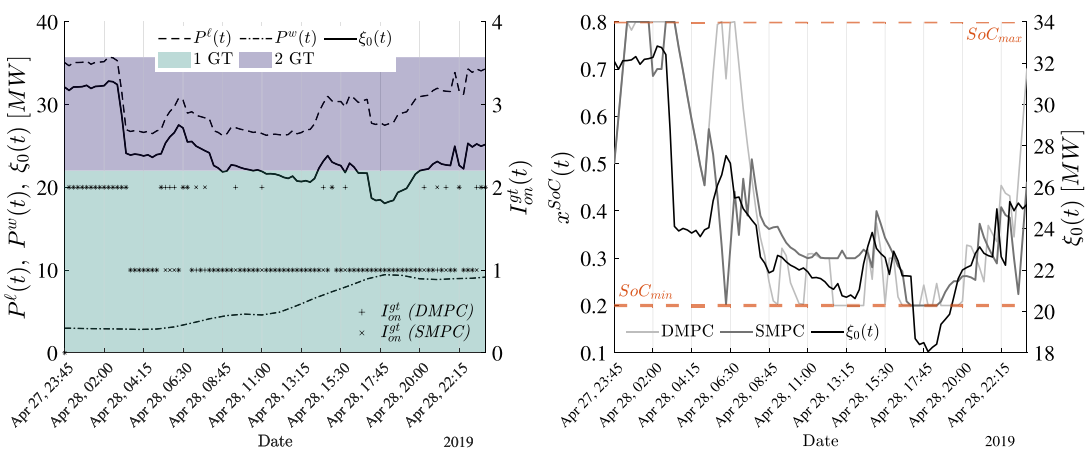

(a) Load, wind power, and net load patterns vs number of on GTs

(b) Net load pattern vs state of charge evolution

Fig. 10. Disturbance and optimal states trajectories (discrete and continuous) with DMPC and SMPC controllers, for the case ML-SD-WU.

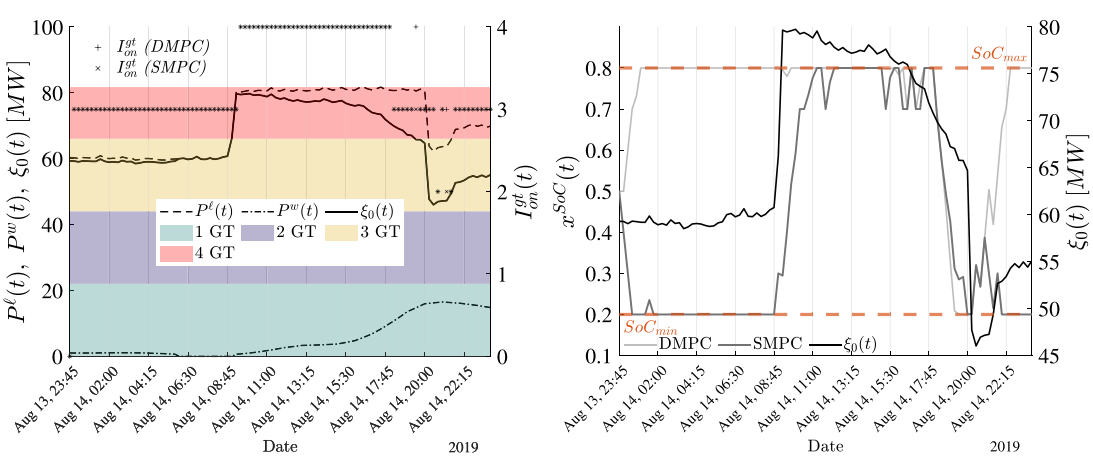

(a) Load, wind power, and net load patterns vs number of on GTs

(b) Net load pattern vs state of charge evolution

Fig. 11. Disturbance and optimal states trajectories (discrete and continuous) with DMPC and SMPC controllers, for the case HL-SUD-WU.

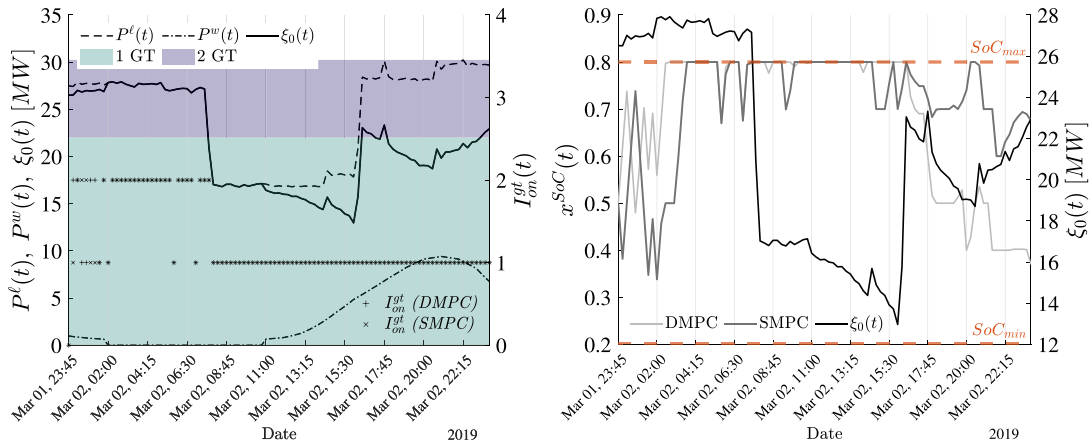

(a) Load, wind power, and net load patterns vs number of on GTs

(b) Net load pattern vs state of charge evolution

Fig. 12. Disturbance and optimal states trajectories (discrete and continuous) with DMPC and SMPC controllers, for the case LL-SDU-WU.

Table 4
HL-SUD-WU KPIs.

KPI	MPC Method		Net
	Mean	*Scn*	
I_c [€]	153,815	152,438	1,377
I_f [tn]	487.72	487.18	0.539
I_{sw} [–]	11	9	2
I_{de} [MWh]	82.16	89.12	−6.961
I_{dg} [%]	0.095	0.070	0.025

Table 5
LL-SDU-WU KPIs.

KPI	MPC Method		Net
	Mean	*Scn*	
I_c [€]	60,633	57,937	2,696
I_f [tn]	170.85	169.97	0.881
I_{sw} [–]	14	11	3
I_{de} [MWh]	28.26	28.24	0.02
I_{dg} [%]	0.317	0.212	0.105

Table 6
HL-SDU-WD KPIs.

KPI	MPC Method		Net
	Mean	*Scn*	
I_c [€]	31,797	27,708	4,089
I_f [tn]	69.97	68.49	1.472
I_{sw} [–]	17	11	6
I_{de} [MWh]	52.45	52.28	0.169
I_{dg} [%]	0.416	0.440	−0.024

SoC trajectories deviate from the first moment while the SMPC chooses to discharge the BESS. As such, and in contrast with the DMPC which chose to have maximum SoC during the early stage, the BESS can later be used to react on the load step up (SU), providing higher efficiency operating points for the additional GT that starts almost simultaneously with this event. However, this action is unavoidably associated with somewhat higher energy dumping compared to the DMPC method, as noticed in Table 4. From Fig. 11(b), we also see that although both methods discharge the BESS equally close to the SD event, the SMPC can better forecast the rapid load increase right afterwards and in contrast with the DMPC, avoids recharging the BESS. In this way, it can get more time with 1 less GT on, resulting in fewer GT startups and degrading the BESS less. The effects are quantified in Table 4.

4.2.5. Case: LL-SDU-WU

Benefits with the proposed SMPC are also noticed from a case with low loading conditions, step transitions from the 2 GTs to 1 GT on regime and vice versa, and wind power ramping up (Fig. 12). From Fig. 12(a) we observe that with both MPC algorithms, we can achieve longer period of times (i.e., in the morning) with 1 GT on while the net load is on the 2 GT regime. Also, from Fig. 12(b) we observe that initially both SoC trajectories follow similar trends, with the one from SMPC presenting deeper discharging. Then, the trajectories deviate again after the second load step variation (step up) where the SMPC trajectory remains at high SoC levels, allowing the single on GT to operate closer to its maximum efficiency point (net load around closer to P_n^{gt}), anticipating for the wind ramping up. In this way, not only lower cost is achieved and fewer GT startups, but also less BESS degradation (Table 5).

4.2.6. Case: HL-SDU-WD

Another interesting case happens when the loading conditions are high but still enough wind power is being generated, resulting in fewer GTs required and almost zero net load (Fig. 13). From Fig. 13(a) we observe once more the capability of the MPC to operate with fewer GTs on, compared to the rule-based benchmark method. In particular, the BESS is used similarly in both methods to discharge power over the period of time right after the load step down, providing the necessary reliability and capacity to the platform and keeping the GTs down for the very low net load values (Fig. 13(b)). However, after the load steps up again, even though both methods result in an oscillatory SoC behavior similarly as in the case *LL-SU-WD*, eventually the trajectories deviate. As a result, the SMPC achieves significant cost and fuel reduction (Table 6).

4.2.7. Case: HL-WD

Finally, similar benefits can be noticed from a case where loading conditions are relatively more stable compared to the rest cases, without large and abrupt steps (Fig. 14). Again, from Fig. 14(a) we can see the superiority of the MPC methods compared to the rule-based one, where the platform can be operated with fewer GTs. Interestingly, the SoC trajectories defined by DMPC and SMPC deviate from the beginning of the day and eventually, when the net load transits from the 1 GT to the 2 GTs regime, the SMPC method manages to hold only 1 GT in operation longer than the DMPC. As a result, significant cost and fuel reductions were achieved again (Table 7).

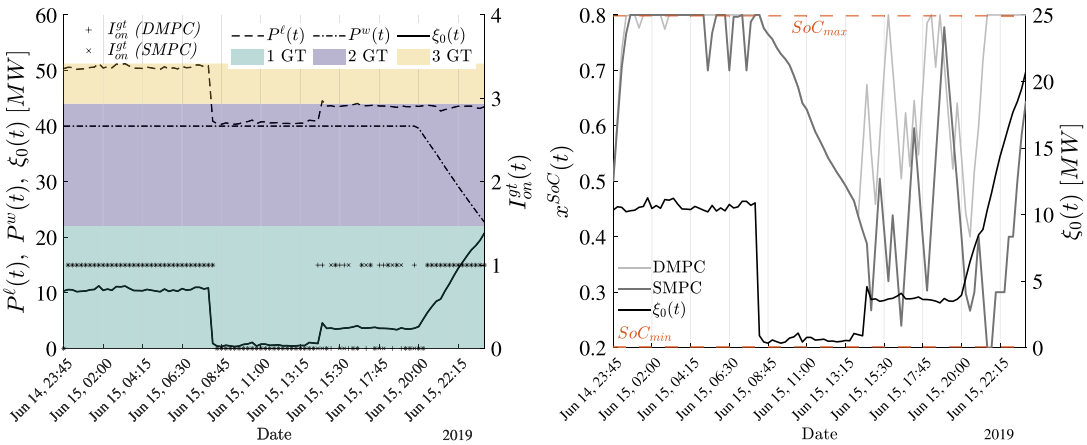

(a) Load, wind power, and net load patterns vs number of on GTs

(b) Net load pattern vs state of charge evolution

Fig. 13. Disturbance and optimal states trajectories (discrete and continuous) with DMPC and SMPC controllers, for the case HL-SDU-WD.

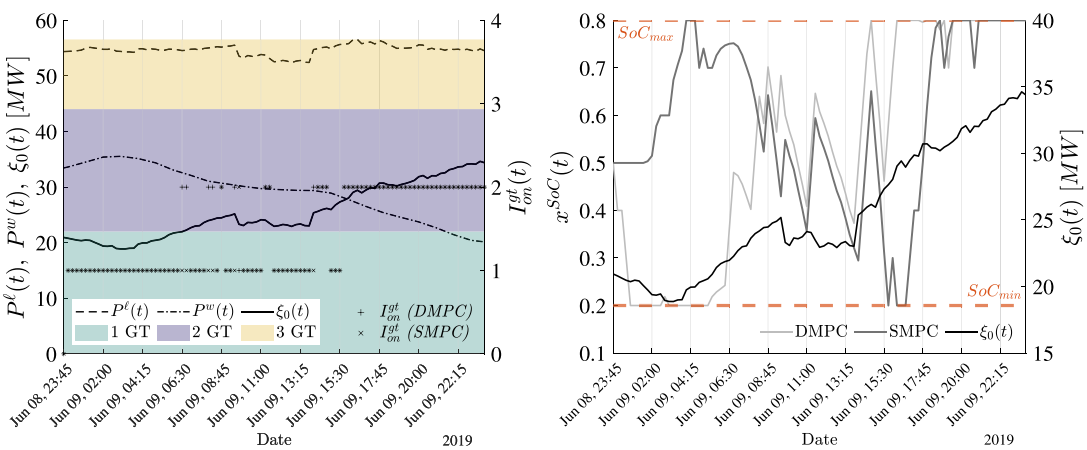

(a) Load, wind power, and net load patterns vs number of on GTs

(b) Net load pattern vs state of charge evolution

Fig. 14. Disturbance and optimal states trajectories (discrete and continuous) with DMPC and SMPC controllers, for the case HL-WD.

Table 7
HL-WD KPIs.

KPI	MPC Method		Net
	Mean	*Scn*	
I_c [€]	69,799	66,510	3,289
I_f [tn]	201.61	198.75	2.870
I_{sw} [–]	14	10	4
I_{de} [MWh]	63.31	63.83	−0.518
I_{dg} [%]	0.375	0.359	0.016

Table 8
Comparison of the DMPC and SMPC methods with relative KPIs.

Case	ΔI_c [%]	ΔI_f [%]	$\Delta I_{on/off}$ [%]
LL-SU-WD	4.338	−0.180	23.53
ML-SD-WU	7.096	2.526	24.00
HL-SUD-WU	0.896	0.111	18.18
LL-SDU-WU	4.447	0.515	21.43
HL-SDU-WD	12.861	2.104	35.29
HL-WD	4.712	1.423	28.57

4.2.8. Cases comparison

The cumulative results for the performance comparison of the DMPC and SMPC methods, for all the cases considered, are given in Table 8. From this table, we can identify the capability of the proposed method to achieve lower fuel consumption, significant cost reduction, and much smoother GT operation, depending on the loading level of the platform and the combination of load and wind power patterns. In particular, we see that the maximum cost reduction (case *HL-SDU-WD*) is associated with the maximum improvement in GT turn ups/downs, while the minimum cost reduction (case *HL-SUD-WU*) is associated with the smallest improvement in GT turn ups/downs. It is also important to clarify that fuel reduction percentages are also equal to the CO_2 emissions reduction percentages, coming from the normal operation of the GTs. However, there are additional environmental benefits resulting from the fewer GT start ups, which are associated with high emissions that would add up to the improvement of the emissions coming from the normal GT operation.

5. Conclusions and future works

It is challenging to operate isolated power systems that integrate renewable sources together with flexible conventional generating units and energy storage, while solving the task efficiently and cost-optimally. This gets even harder for industrial systems or small scale isolated grids where the load intermittency is increased compared to large power systems where load aggregation has a smoothing effect. Short-term abrupt step variations combined with the stochastic nature of renewable sources make it hard to accurately forecast the near future power imbalance. Thus, the power scheduling solution from the energy management system may be sub-optimal. In addition, the existence of binary operational status of conventional thermal units and the multiple conflicting objectives pose an additional challenge to preforming optimal energy management.

This paper proposed a Stochastic Model Predictive Control scheme aimed at solving the EMS problem under uncertainty for isolated power systems that are characterized by abrupt load variations and lack of future events information. The developed controller is designed to solve an optimal control problem on a rolling horizon basis, using stochastic mixed-integer linear programming and considering the minimization of operational costs, battery degradation, and dumped energy simultaneously. The proposed EMS framework integrates a data-driven mechanism to represent future uncertainty by means of quantile regression and scenario generation, providing useful information for the expected uncertainty bounds over the load and renewable generation. With the proposed probabilistic forecasting framework, significant skill score improvement was achieved for both load forecasts (91.50%) and wind power forecasts (90.50%). This made it possible to better anticipate near-future irregular events just by using past information.

We thus considered the specific case study of an offshore O&G platform that integrates wind power. The performance of the proposed algorithm was then evaluated and benchmarked against a deterministic version to assess the benefits of making the optimization problem stochastic. For this reason, several case studies capturing the high variation of loading conditions (characterizing O&G platforms) and the intermittency of wind power were considered. The results showed that, under the proposed SMPC-EMS, in all the patterns examined, better planning of the resources could be achieved leading to daily operational cost savings up to 12.86%, fuel consumption and emissions reduction from normal GT operation up to 2.56%, and less switching of the GTs up to 35.29%.

Even though the proposed SMPC-EMS deals with the optimal techno-economic operation of the isolated grid, it does not explicitly consider operational constraints related to the smaller time-scale stability of the system when rapid net load variations occur. Such a limitation could be overcome by integrating adaptive state of charge limits, ensuring the additional provision of ancillary services by the energy storage system, supporting the local grid. The proposed method could be easily adapted to other cases of isolated power systems (i.e., any kind of industrial plants or small-scale physical islands) that integrate various and multiple kinds of renewable sources (i.e., solar energy) by repurposing the QRF models on the corresponding datasets and including more stochastic scenarios representing disturbances from each random variable, to cover a possibly more diverse situation.

CRediT authorship contribution statement

Spyridon Chapaloglou: Conceptualization, Methodology, Validation, Visualization, Software, Writing – original draft. **Damiano Varagnolo:** Supervision, Writing – review & editing. **Francesco Marra:** Supervision, Writing – review & editing. **Elisabetta Tedeschi:** Supervision, Writing – review & editing.

Table 9
Nomenclature.

Description	Symbol
Random Forest	
Tree in set of trees bag	$t \in \mathcal{T}$
Lead time in prediction horizon	$k \in \mathcal{K}$
Observations in dataset	$Y_j,\ j = 1, \dots, N$
Predictor (input feature)	$x = [P_t, P_{t-1}, \dots, P_{t-L}]$
Power value at time t	P_t
Leaf set of values of a tree t containing predictor x	$x \in S_t(x)$
Induced weight of tree t for observation j	$w_{tj}(x)$
Induced weight of observation j	$w_j(x)$
Mean response value of the random forest	$\hat{y}_j(x)$
Percentile	τ
Quantile of predictor x	$Q_\tau(x)$
Estimated prediction interval given x	$\hat{\alpha}(x)$
Observation value (input predictor)	$x \in \mathcal{X}$
Future values (data)	$y_{t+k\|t}$
Scenario generated	$i \in \mathcal{N}_s$
Response value (prediction)	$\hat{y}_{t+k\|t}$
Response value (prediction) for scenario i	$\hat{y}^{(i)}_{t+k\|t}$
Power consumption random variable	P^{ℓ}
Wind power random variable	P^{w}
SMPC	
Piecewise linear approximations	$p = 1, \dots, N_{pwl}$
Set of available synchronous generators	$g = 1, \dots, N_g$
Set of scenarios	$\omega = 1, \dots, N_\omega$
Set of lead times for the forecasting models	$k = 1, \dots, \|\mathcal{K}\|$
Fuel curve X data values (P^{gt} [MW])	$\mathbf{D}^{gt}_P$
Fuel curve Y data values (f^{gt} [kg/MWh])	$\mathbf{D}^{gt}_f$
Fuel curve	$\mathcal{F}_{fuel}$
Battery degradation curve X values	$\mathbf{D}^{deg}_{dod}$
Battery degradation curve Y values	$\mathbf{D}^{deg}_{cyc}$
Battery degradation curve	$\mathcal{F}_{deg}$
State of charge	x^{SoC}
GT status	$\mathbf{x}^{gt}_{1:N_g}$
Control input	$\mathbf{u}$
Charging power	P^{ch}
Discharging power	P^{dis}
GT turn ON command	$b^{gt,on}_g$
GT turn OFF command	$b^{gt,off}_g$
GT power	P^{gt}
Random disturbance	ξ
Random variable at time t	$P^p_{t+k},\ p = \{\ell, w\}$
Estimated inverse conditional CDF	$\hat{F}^{p\,-1}_{t+k\|t}\left(P^p_{t+k} \mid x\right)$
Inverse normal CDF	Φ^{-1}

Declaration of competing interest

The authors declare that they have no known competing financial interests or personal relationships that could have appeared to influence the work reported in this paper.

Appendix A

See Tables 9 and 10.

Appendix B

List of sets used in the proposed models:

1. $p = 1, \dots, N_{pwl}$: points used in the piecewise linear approximations of non-linear functions
2. $g = 1, \dots, N_g$: set of available gas turbines (conventional generators)
3. $\omega = 1, \dots, N_\omega$: set of scenarios
4. $k = 1, \dots, |\mathcal{K}|$: set of lead times for the forecasting models

List of sets of data points:

1. $\mathbf{D}^{gt}_P = \left[D^{gt}_{P,1}, \dots, D^{gt}_{P,N_{pwl}}\right]^T$: fuel curve X data values (P^{gt} [MW])

Table 10
Parameters.

Parameter	Symbol	Value	Units
Sets			
Gas Turbines	N_g	4	[–]
Scenarios	N_ω	10	[–]
PWL points	N_{pwl}	11	[–]
Prediction horizon (SMPC)	$\lvert \mathcal{K} \rvert$	6	[–]
Non-linear curves			
Fuel curve coefficient	α_f	0.5109	[–]
Fuel curve coefficient	β_f	−20.933	[–]
Fuel curve coefficient	γ_f	433.83	[–]
Degradation curve coefficient	k_0	1591.1	[–]
Degradation curve coefficient	k_1	2.089	[–]
BESS			
Max battery power	$\overline{P}^b$	5	[MW]
Battery capacity	$\overline{E}^b$	10	[MWh]
Max state of charge	SoC_{max}	0.8	[p.u.]
Min state of charge	SoC_{min}	0.2	[p.u.]
Charging efficiency	η_{ch}	0.95	[p.u.]
Discharging efficiency	η_{dis}	0.95	[p.u.]
GT			
Nominal GT power	P_n^{gt}	20.200	[MW]
Max GT power	$\overline{P}^{gt}$	22.018	[MW]
Min GT power	$\underline{P}^{gt}$	4.040	[MW]
GT ramping rate	RR	22.018	[MW/15 min]
Spinning reserve	s_r	5	[%]
Idling (no-load) fuel consumption	c_f^{idle}	1,679	[kg/h]
cost coefficients			
Fuel cost	c_f	0.2979	[€/kg]
Startup cost	c_{gt}^{str}	1,217	[€/startup]
Fixed on cost	c_{gt}^{on}	5,000	[€/on time]
Battery replacement cost	$c_{b,rpl}$	445,000	[€]
Battery residual cost	$c_{b,res}$	44,500	[€]
Energy dumping cost	$c_{b,res}$	1,000	[€/MW]
Wind Turbine Power Curve			
Cut in speed	w_{ci}	3	$\left[\frac{m}{s}\right]$
Cut off speed	w_{co}	25	$\left[\frac{m}{s}\right]$
Rated wind speed	w_n	12	$\left[\frac{m}{s}\right]$
Rated power	P_n^w	8	[MW]
Wind turbines	N_w	5	[–]
Simulation time step	T_s	15	[min]
Case studies duration	T_t	24	[h]

2. $\mathbf{D}_f^{gt} = \left[D_{f,1}^{gt}, \dots, D_{f,N_{pwl}}^{gt}\right]^T$: fuel curve Y data values (f^{gt} [kg/MWh])
3. $\mathbf{D}_f^{gt} = \mathcal{F}_{fuel}(\mathbf{D}_P^{gt})$ transformation (fuel curve)
4. $\mathcal{F}_{fuel}(x) = \alpha_f x + \beta_f x + \gamma_f$ fuel curve definition
5. $\mathbf{D}_{dod}^{deg} = \left[D_{dod,1}^{deg}, \dots, D_{dod,N_{pwl}}^{deg}\right]^T$: battery degradation curve X values
6. $\mathbf{D}_{cyc}^{deg} = \left[D_{cyc,1}^{deg}, \dots, D_{cyc,N_{pwl}}^{deg}\right]^T$: battery degradation curve Y values
7. $\mathbf{D}_{cyc}^{deg} = \mathcal{F}_{deg}(\mathbf{D}_{dod}^{deg})$ transformation (degradation curve)
8. $\mathcal{F}_{deg}(x) = \frac{100}{k_0 x^{-k_1}}$ degradation curve definition

Fuel curve PWL approximation

$$\mathbb{1}^T_{\{1:N_{pwl}\}} \cdot \mathbf{w}_{k,\omega,g}^{fuel} = x_{k,\omega,g}^{gt} \tag{64}$$

$$w_{k,\omega,g,1}^{fuel} \le \lambda_{k,\omega,g,1}^{fuel} \tag{65}$$

$$w_{k,\omega,g,p}^{fuel} \le \lambda_{k,\omega,g,p-1}^{fuel} + \lambda_{k,\omega,g,p}^{fuel} \tag{66}$$

$$w_{k,\omega,g,N_{pwl}}^{fuel} \le \lambda_{k,\omega,g,N_{pwl}-1}^{fuel} \tag{67}$$

$$\mathbb{1}^T_{\{1:N_{pwl}-1\}} \cdot \lambda_{k,\omega,g}^{fuel} = x_{k,\omega,g}^{gt} \tag{68}$$

We define $\boldsymbol{B}_\omega$ as a square matrix of dimension $\lvert \mathcal{K} \rvert$ as

$$\boldsymbol{B}_\omega = \begin{bmatrix} 1 & 0 \cdots & 0 \\ 1 & 1 \cdots & 0 \\ & \vdots & \\ 1 & 1 \cdots & 1 \end{bmatrix} \quad \forall\, \omega = 1, \dots, N_\omega \tag{69}$$

and

$$\boldsymbol{B} = \begin{bmatrix} \boldsymbol{B}_1 & 0 & 0 \\ 0 & \ddots & 0 \\ 0 & 0 & \boldsymbol{B}_{N_\omega} \end{bmatrix} \tag{70}$$

Degradation curve PWL approximation

$$\mathbb{1}^T_{\{1:N_{pwl}\}} \cdot \mathbf{w}_{k,\omega}^{deg} = 1 \tag{71}$$

$$w_{k,\omega,1}^{deg} \le \lambda_{k,\omega,1}^{deg} \tag{72}$$

$$w_{k,\omega,p}^{deg} \le \lambda_{k,\omega,p-1}^{deg} + \lambda_{k,\omega,p}^{deg} \tag{73}$$

$$w_{k,\omega,N_{pwl}}^{deg} \le \lambda_{k,\omega,N_{pwl}-1}^{deg} \tag{74}$$

$$\mathbb{1}^T_{\{1:N_{pwl}-1\}} \cdot \lambda_{k,\omega}^{deg} = 1 \tag{75}$$

References

[1] Machlev R, Zargari N, Chowdhury NR, Belikov J, Levron Y. A review of optimal control methods for energy storage systems - energy trading, energy balancing and electric vehicles. J Energy Storage 2020;32:101787. http://dx.doi.org/10.1016/j.est.2020.101787, URL http://www.sciencedirect.com/science/article/pii/S2352152X20316248.

[2] Itiki R, Di Santo SG, Itiki C, Manjrekar M, Chowdhury BH. A comprehensive review and proposed architecture for offshore power system. Int J Electr Power Energy Syst 2019;111:79–92. http://dx.doi.org/10.1016/j.ijepes.2019.04.008, URL http://www.sciencedirect.com/science/article/pii/S014206151930095X.

[3] Settemsdal S, Barstad L, Voss W. Hybrid power plants can help decarbonize offshore drilling rigs and vessels. Endeavor Bus Media 2020;(Offshore):4.

[4] Abidi MG, Ben Smida M, Khalgui M, Li Z, Wu N. Multi-agent oriented solution for forecasting-based control strategy with load priority of microgrids in an island mode – Case study: Tunisian petroleum platform. Electr Power Syst Res 2017;152:411–23. http://dx.doi.org/10.1016/j.epsr.2017.07.013, URL https://linkinghub.elsevier.com/retrieve/pii/S0378779617302985.

[5] Pavković D, Sedić A, Guzović Z. Oil drilling rig diesel power-plant fuel efficiency improvement potentials through rule-based generator scheduling and utilization of battery energy storage system. Energy Convers Manage 2016;121:194–211. http://dx.doi.org/10.1016/j.enconman.2016.05.022, URL https://linkinghub.elsevier.com/retrieve/pii/S0196890416303909.

[6] Jafari M, Botterud A, Sakti A. Estimating revenues from offshore wind-storage systems: The importance of advanced battery models. Appl Energy 2020;276:115417. http://dx.doi.org/10.1016/j.apenergy.2020.115417, URL https://www.sciencedirect.com/science/article/pii/S0306261920309296.

[7] Anglani N, Oriti G, Colombini M. Optimized energy management system to reduce fuel consumption in remote military microgrids, 9.

[8] Berrueta A, Heck M, Jantsch M, Ursúa A, Sanchis P. Combined dynamic programming and region-elimination technique algorithm for optimal sizing and management of lithium-ion batteries for photovoltaic plants. Appl Energy 2018;228:1–11. http://dx.doi.org/10.1016/j.apenergy.2018.06.060, URL https://linkinghub.elsevier.com/retrieve/pii/S0306261918309279.

[9] Roslan MF, Hannan MA, Jern Ker P, Begum RA, Indra Mahlia T, Dong ZY. Scheduling controller for microgrids energy management system using optimization algorithm in achieving cost saving and emission reduction. Appl Energy 2021;292:116883. http://dx.doi.org/10.1016/j.apenergy.2021.116883, URL https://www.sciencedirect.com/science/article/pii/S0306261921003718.

[10] Restrepo M, Cañizares CA, Simpson-Porco JW, Su P, Taruc J. Optimization- and rule-based energy management systems at the Canadian renewable energy laboratory microgrid facility. Appl Energy 2021;290:116760. http://dx.doi.org/10.1016/j.apenergy.2021.116760, URL https://www.sciencedirect.com/science/article/pii/S0306261921002671.

[11] Zhang Y, Wang J, Wang X. Review on probabilistic forecasting of wind power generation. Renew Sustain Energy Rev 2014;32:255–70. http://dx.doi.org/10.1016/j.rser.2014.01.033, URL https://www.sciencedirect.com/science/article/pii/S1364032114000446.

[12] Worsnop RP, Scheuerer M, Hamill TM, Lundquist JK. Generating wind power scenarios for probabilistic ramp event prediction using multivariate statistical post-processing. Wind Energy Sci 2018;3(1):371–93. http://dx.doi.org/10.5194/wes-3-371-2018, URL https://www.wind-energ-sci.net/3/371/2018/.

[13] Parisio A, Glielmo L. Energy efficient microgrid management using model predictive control. In: 2011 50th IEEE conference on decision and control and european control conference. 2011, p. 5449–54. http://dx.doi.org/10.1109/CDC.2011.6161246, ISSN: 0743-1546.

[14] Parisio A, Fabietti L, Molinari M, Varagnolo D, Johansson KH. Control of HVAC systems via scenario-based explicit MPC. In: 53rd IEEE conference on decision and control. Los Angeles, CA, USA: IEEE; 2014, p. 5201–7. http://dx.doi.org/10.1109/CDC.2014.7040202, URL http://ieeexplore.ieee.org/document/7040202/.

[15] Bø TI, Vaktskjold E, Pedersen E, Mo O. Model predictive control of marine power plants with gas engines and battery. IEEE Access 2019;7:15706–21. http://dx.doi.org/10.1109/ACCESS.2019.2895163, Conference Name: IEEE Access.

[16] Richards A, How J. Mixed-integer programming for control. In: Proceedings of the 2005, American control conference, 2005. Portland, OR, USA: IEEE; 2005, p. 2676–83. http://dx.doi.org/10.1109/ACC.2005.1470372, URL http://ieeexplore.ieee.org/document/1470372/.

[17] Parisio A, Rikos E, Glielmo L. A model predictive control approach to microgrid operation optimization. IEEE Trans Control Syst Technol 2014;22(5):1813–27. http://dx.doi.org/10.1109/TCST.2013.2295737, Conference Name: IEEE Transactions on Control Systems Technology.

[18] Cardoso G, Brouhard T, DeForest N, Wang D, Heleno M, Kotzur L. Battery aging in multi-energy microgrid design using mixed integer linear programming. Appl Energy 2018;231:1059–69. http://dx.doi.org/10.1016/j.apenergy.2018.09.185, URL https://linkinghub.elsevier.com/retrieve/pii/S0306261918315058.

[19] Parisio A, Rikos E, Glielmo L. Stochastic model predictive control for economic/environmental operation management of microgrids: An experimental case study. J Process Control 2016;43:24–37. http://dx.doi.org/10.1016/j.jprocont.2016.04.008, URL https://www.sciencedirect.com/science/article/pii/S0959152416300324.

[20] Silvente J, Kopanos GM, Dua V, Papageorgiou LG. A rolling horizon approach for optimal management of microgrids under stochastic uncertainty. Chem Eng Res Des 2018;131:293–317. http://dx.doi.org/10.1016/j.cherd.2017.09.013, URL https://www.sciencedirect.com/science/article/pii/S0263876217304665.

[21] Tang C, Wang Y, Xu J, Sun Y, Zhang B. Efficient scenario generation of multiple renewable power plants considering spatial and temporal correlations. Appl Energy 2018;221:348–57. http://dx.doi.org/10.1016/j.apenergy.2018.03.082, URL https://linkinghub.elsevier.com/retrieve/pii/S0306261918304203.

[22] Camal S, Teng F, Michiorri A, Kariniotakis G, Badesa L. Scenario generation of aggregated wind, photovoltaics and small hydro production for power systems applications. Appl Energy 2019;242:1396–406. http://dx.doi.org/10.1016/j.apenergy.2019.03.112, URL https://linkinghub.elsevier.com/retrieve/pii/S0306261919305203.

[23] Lei Y, Wang D, Jia H, Chen J, Li J, Song Y, et al. Multi-objective stochastic expansion planning based on multi-dimensional correlation scenario generation method for regional integrated energy system integrated renewable energy. Appl Energy 2020;276:115395. http://dx.doi.org/10.1016/j.apenergy.2020.115395, URL https://www.sciencedirect.com/science/article/pii/S0306261920309077.

[24] Hafiz F, Rodrigo de Queiroz A, Fajri P, Husain I. Energy management and optimal storage sizing for a shared community: A multi-stage stochastic programming approach. Appl Energy 2019;236:42–54. http://dx.doi.org/10.1016/j.apenergy.2018.11.080, URL https://www.sciencedirect.com/science/article/pii/S0306261918317963.

[25] van der Meer D, Wang GC, Munkhammar J. An alternative optimal strategy for stochastic model predictive control of a residential battery energy management system with solar photovoltaic. Appl Energy 2021;283:116289. http://dx.doi.org/10.1016/j.apenergy.2020.116289, URL https://linkinghub.elsevier.com/retrieve/pii/S0306261920316767.

[26] Talari S, Yazdaninejad M, Haghifam M-R. Stochastic-based scheduling of the microgrid operation including wind turbines, photovoltaic cells, energy storages and responsive loads. Transm Distribution IET Gener 2015;9(12):1498–509. http://dx.doi.org/10.1049/iet-gtd.2014.0040, Conference Name: Transmission Distribution IET Generation.

[27] Giaouris D, Papadopoulos AI, Patsios C, Walker S, Ziogou C, Taylor P, et al. A systems approach for management of microgrids considering multiple energy carriers, stochastic loads, forecasting and demand side response. Appl Energy 2018;226:546–59. http://dx.doi.org/10.1016/j.apenergy.2018.05.113, URL https://www.sciencedirect.com/science/article/pii/S030626191830833X.

[28] Silva JAA, López JC, Arias NBn, Rider MJ, da Silva LCP. An optimal stochastic energy management system for resilient microgrids. Appl Energy 2021;300:117435. http://dx.doi.org/10.1016/j.apenergy.2021.117435, URL https://www.sciencedirect.com/science/article/pii/S0306261921008254.

[29] Torossian L, Picheny V, Faivre R, Garivier A. A review on quantile regression for stochastic computer experiments. 2019, URL https://hal.archives-ouvertes.fr/hal-02010735.

[30] Correa-Florez CA, Gerossier A, Michiorri A, Kariniotakis G. Stochastic operation of home energy management systems including battery cycling. Appl Energy 2018;225:1205–18. http://dx.doi.org/10.1016/j.apenergy.2018.04.130, URL https://linkinghub.elsevier.com/retrieve/pii/S0306261918306597.

[31] Poolla C, Ishihara AK, Milito R. Designing near-optimal policies for energy management in a stochastic environment. Appl Energy 2019;242:1725–37. http://dx.doi.org/10.1016/j.apenergy.2019.01.228, URL https://www.sciencedirect.com/science/article/pii/S0306261919302570.

[32] Han D, Lee JH. Two-stage stochastic programming formulation for optimal design and operation of multi-microgrid system using data-based modeling of renewable energy sources. Appl Energy 2021;291:116830. http://dx.doi.org/10.1016/j.apenergy.2021.116830, URL https://www.sciencedirect.com/science/article/pii/S0306261921003299.

[33] Parisio A, Varagnolo D, Molinari M, Pattarello G, Fabietti L, Johansson KH. Implementation of a scenario-based MPC for HVAC systems: An experimental case study. IFAC Proc Vol 2014;47(3):599–605. http://dx.doi.org/10.3182/20140824-6-ZA-1003.02629, URL https://linkinghub.elsevier.com/retrieve/pii/S1474667016416800.

[34] Parisio A, Molinari M, Varagnolo D, Johansson KH. A scenario-based predictive control approach to building HVAC management systems. In: 2013 IEEE international conference on automation science and engineering. Madison, WI, USA: IEEE; 2013, p. 428–35. http://dx.doi.org/10.1109/CoASE.2013.6654024, URL http://ieeexplore.ieee.org/document/6654024/.

[35] Parisio A, Varagnolo D, Risberg D, Pattarello G, Molinari M, Johansson KH. Randomized model predictive control for HVAC systems. In: Proceedings of the 5th ACM workshop on embedded systems for energy-efficient buildings. Roma, Italy: ACM Press; 2013, p. 1–8. http://dx.doi.org/10.1145/2528282.2528299, URL http://dl.acm.org/citation.cfm?doid=2528282.2528299.

[36] Patrinos P, Trimboli S, Bemporad A. Stochastic MPC for real-time market-based optimal power dispatch. In: IEEE Conference on decision and control and european control conference. Orlando, FL, USA: IEEE; 2011, p. 7111–6. http://dx.doi.org/10.1109/CDC.2011.6160798, URL http://ieeexplore.ieee.org/document/6160798/.

[37] Meinshausen N. Quantile regression forests. J Mach Learn Res 2006;7:983–99.

[38] Golestaneh F, Gooi HB, Pinson P. Generation and evaluation of space–time trajectories of photovoltaic power. Appl Energy 2016;176:80–91. http://dx.doi.org/10.1016/j.apenergy.2016.05.025, URL https://linkinghub.elsevier.com/retrieve/pii/S0306261916306079.

[39] Zhang S, Wang Y, Zhang Y, Wang D, Zhang N. Load probability density forecasting by transforming and combining quantile forecasts. Appl Energy 2020;277:115600. http://dx.doi.org/10.1016/j.apenergy.2020.115600, URL https://www.sciencedirect.com/science/article/pii/S0306261920311065.

[40] D'Ambrosio C, Lodi A, Martello S. Piecewise linear approximation of functions of two variables in MILP models. Oper Res Lett 2010;38(1):39–46. http://dx.doi.org/10.1016/j.orl.2009.09.005, URL https://www.sciencedirect.com/science/article/pii/S0167637709001072.

[41] Wang Y, Zhou Z, Botterud A, Zhang K, Ding Q. Stochastic coordinated operation of wind and battery energy storage system considering battery degradation. J Mod Power Syst Clean Energy 2016;4(4):581–92. http://dx.doi.org/10.1007/s40565-016-0238-z, URL http://link.springer.com/10.1007/s40565-016-0238-z.

[42] Pinson P, Madsen H, Nielsen HA, Papaefthymiou G, Klöckl B. From probabilistic forecasts to statistical scenarios of short-term wind power production. Wind Energy 2009;12(1):51–62. http://dx.doi.org/10.1002/we.284, _eprint: https://onlinelibrary.wiley.com/doi/pdf/10.1002/we.284, URL https://onlinelibrary.wiley.com/doi/abs/10.1002/we.284.

[43] Papaefthymiou G, Kurowicka D. Using copulas for modeling stochastic dependence in power system uncertainty analysis. IEEE Trans Power Syst 2009;24(1):40–9. http://dx.doi.org/10.1109/TPWRS.2008.2004728, Conference Name: IEEE Transactions on Power Systems.

[44] Pfenninger S, Staffell I. Long-term patterns of European PV output using 30 years of validated hourly reanalysis and satellite data. Energy 2016;114:1251–65. http://dx.doi.org/10.1016/j.energy.2016.08.060, URL https://www.sciencedirect.com/science/article/pii/S0360544216311744.

[45] Staffell I, Pfenninger S. Using bias-corrected reanalysis to simulate current and future wind power output. Energy 2016;114:1224–39. http://dx.doi.org/10.1016/j.energy.2016.08.068, URL https://www.sciencedirect.com/science/article/pii/S0360544216311811.

[46] Pinson P, Girard R. Evaluating the quality of scenarios of short-term wind power generation. Appl Energy 2012;96:12–20. http://dx.doi.org/10.1016/j.apenergy.2011.11.004, URL https://linkinghub.elsevier.com/retrieve/pii/S0306261911006994.

[47] Bjerregård MB, Møller JK, Madsen H. An introduction to multivariate probabilistic forecast evaluation. Energy AI 2021;4:100058. http://dx.doi.org/10.1016/j.egyai.2021.100058, URL https://www.sciencedirect.com/science/article/pii/S2666546821000124.

[48] Yang D. A universal benchmarking method for probabilistic solar irradiance forecasting. Sol Energy 2019;184:410–6. http://dx.doi.org/10.1016/j.solener.2019.04.018, URL https://www.sciencedirect.com/science/article/pii/S0038092X19303457.